New Approaches to Electrocaloric-Based Multilayer Cooling

Sergey Karmanenko, Alexander Semenov, Antonina Dedyk, Andrey Es'kov, Alexey Ivanov, Pavel Beliavskiy, Yulia Pavlova, Andrey Nikitin, Ivan Starkov, Alexander Starkov and Oleg Pakhomov

1 Introduction

The research and development works directed to a creation of solid state coolers and refrigerators based on the electrocaloric effect have been initiated in various countries, mainly in USA and USSR, in the 70s of the last century [39, 43]. The goal of these works was formed as a creation of microcryogenic cooling systems for infrared radiation receivers for space optoelectronic systems. The following principles of R&D works were formulated at the initial stage:

- The mechanical thermal keys were used for the connection between active electrocaloric elements in order to decrease the temperature of cooling object.
- The temperature decrease in active element was achieved in the process of electric field action on ferroelectric capacitor and the cooling of gas carrier flowing through it.
- Thermodynamic cycle of gas carrier with electrocaloric active elements should be similar to analogical cycles of the gas expansion processes in vapor-compression refrigerators.

At a later date these principles were used in such developments as [42], where various modifications of completely solid state electrocaloric refrigerators featuring with thermal keys were considered. That approach to the creation of the

S. Karmanenko · A. Semenov · A. Dedyk · A. Es'kov · A. Ivanov · P. Beliavskiy · Y. Pavlova · A. Nikitin
St. Petersburg State Electrotechnical University (LETI), St. Petersburg, Russia

I. Starkov
Institute for Microelectronics, Vienna University of Technology, Vienna, Austria

A. Starkov · O. Pakhomov (✉)
National Research University of Information Technologies, Mechanics and Optics (ITMO), St. Petersburg, Russia
e-mail: oleg.cryogenics@gmail.com

T. Correia and Q. Zhang (eds.), *Electrocaloric Materials*, Engineering Materials 34, DOI: 10.1007/978-3-642-40264-7_8,
© Springer-Verlag Berlin Heidelberg 2014

refrigerating device is based on quasi-static method, where thermodynamic cooling cycle is considered as the serial set of reverse equilibrium processes.

In conventional vapor-compression refrigerators the thermal processes is realized in stationary regime, however at last years the novel refrigerating principles based on dynamic thermal processes have found useful application, such as «Pulse Tube Cryocooler», «Vortex tube», «Gifford–McMahon Cryocooler». Also, quasi-stationary thermal processes take place in Stirling cryocoolers, which use two working body—gas and solid material of the regenerator [2].

In the papers published after 2006 [9, 20, 27] there were presented some variants of new generation of dynamical electrocaloric devices without application of mechanical thermal keys and gas carrier. In the mentioned papers the layered ferroelectric structures were proposed as heat transferring line, where thermoelectric Pelitier elements, liquid crystal films or heat transferring elements are used. Describing the last structure, the authors shown that at the defined conditions ferroelectric layered structure should work as highly efficient solid-state heat pump.

The proposed type of thermal devices based on the solid layered structures possesses a set of principal features. These are the matched dynamical character of switching processes in every ferroelectric layer and a presence of thermal interaction of heat responses across the layered structure. The dynamical matching of electrocaloric and elastocaloric effects give the parametric amplification both electrocaloric response and heat flux in the layered structure [9].

The novel type of EC refrigerator is similar to cryogenic dynamic refrigerator and less resembling than to the quasi-static thermal device. Therefore to create the new generation of EC devices it is necessary to investigate an electrocaloric response at exposure of various structure (harmonic signal, rectangular pulses or the action of other dynamic forms) electric field and study dynamical characteristic of various ferroelectric materials. Theoretical efficiency of multilayer cooling structures could be estimated just by analysis of interfering dynamical processes in adjoining EC elements.

2 Theoretical Basis of Modern Electrocaloric-Based Cooling Structures

2.1 Efficiency of Electrocaloric-Based Cooling in Quasi-Static Approximation

Solid-state converters of thermal energy and energy-saving technologies of cooling form an important trend in research and development at many laboratories and companies during the last few decades. The main advantage of solid-state cooling is determined by a considerably higher density of solids as compared to vapor and gas in vapor-compression systems. The change in the entropy per unit volume in solid materials is 6–8 times higher than in gases [4], which makes it possible to

considerably reduce the size of refrigerators and to produce miniature thermal energy converters.

Among thermal physical phenomena in solids, the conversion of thermal energy in a ferroelectric material [3], occurring as a result of the pyroelectric and electrocaloric effects, has special importance. The ferroelectric converters have high efficiency due to the fact that heating and cooling of the coolant are practically reversible thermodynamic cycles [3, 35, 50].

Until recently it was assumed that the electrocaloric method of cooling has a low efficiency and not suitable for coolers [28, 35]. However, the last theoretical and experimental advances in material science [11, 15, 20, 27, 45] proved that film capacitors based on perovskite, relaxant, and polymer materials [33] can ensure a thermal effect exceeding 10 K in a single switching. At the same time, the key direction in the development of a solid-state cooler is the construction of the effective thermodynamic cycle of a system of thermal converters. Thermodynamic analysis of thermal processes in a ferroelectric energy converter was considered, for example, in [17, 41]. However, the sequence (dynamics) of switching of EC elements and the shape of the applied voltage (which has not been considered before as far as we know) are very important to estimate the effectiveness of converter operation.

An important circumstance for choosing the operation conditions for a thermal line is setting of the temperature interval in which effective conversion of heat occurs. Estimates obtained in [31] show that in the vicinity of the phase transition, the efficiency of conversion of thermal energy into electric energy tends to the efficiency of the Carnot cycle. Which temperature range is most effective for EC cooling in a capacitor? This question will be considered in this chapter devoted to the thermodynamic estimation of the efficiency of conversion of electric energy in a solid-state cooling line including ferroelectric capacitors under the action of electric pulses.

In our publications [10, 36], we analyzed thermal processes in a cooling line including two EC elements and three thermal conductors. Numerical simulation was performed using the finite element method. As a result, it was shown that a steady-state temperature regime is formed in the solid-state cooling line under investigation, and the temperature gradient is directed from the source of the sink of thermal energy. When ferroelectric capacitors based on $Ba_xSr_{1-x}TiO_3$ barium–strontium titanate (BST) ceramic is used, the temperature difference may attain 25 K in the case of perfect heat removal. The necessary condition for the operation of a solid-state line is matching of the operation modes of the capacitors at the maximum of the derivative of electric polarization (dP/dT) or permittivity ($d\varepsilon/dT$) with respect to temperature.

Figure 1 shows the temperature dependence of the permittivity of the BST ceramic and its derivative with respect to temperature. A ferroelectric capacitor operates most effectively as an EC element in the paraelectric phase at the temperature corresponding to the extremum on the $d\varepsilon/dT(T)$ dependence. Therefore, it is expedient to use ferroelectric capacitors for which the temperature corresponding to the extremum on the $d\varepsilon/dT(T)$ dependence increases in the source-sink direction.

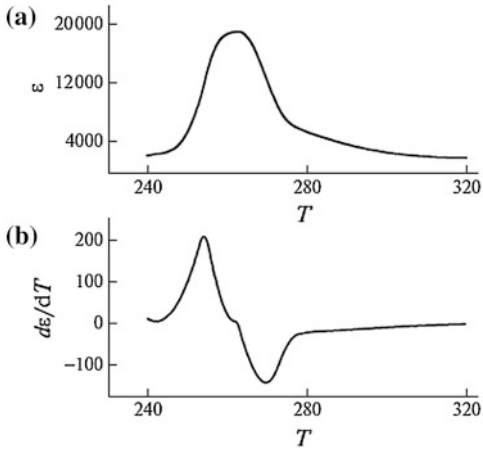

Fig. 1 The temperature dependences of permittivity **a** and its derivative **b** in ferroelectric capacitor based on BST ceramic

We will consider the thermodynamic efficiency of EC cooling in steady state. For a correct analysis we make the following assumptions are valid for quasi-static processes:

- Make-and-break of EC elements is performed by applying periodic voltage pulses. The operation of a cooling structure requires a time shift between sequences of pulses supplied to the first and second EC elements. The time shift in the operation of capacitors is multiple to the thermal constant defined as

$$\tau = \frac{L^2 \rho C}{\lambda},$$

  where L, ρ, C, and λ are the length (thickness), density, heat capacity, and thermal conductivity of the ferroelectric.
- Charging and discharging occur either adiabatically, or isothermally. The thermal and electrical duration of the pulse front in these cases may differ by several orders of magnitude. If the front duration is much smaller than the thermal constant of the transition from one energy state to another, charging (discharging) occurs adiabatically. If the charging time considerably exceeds the time constant, the charging (discharging) process occurs isothermally.
- Heat loss and dissipation of electric energy are negligibly small and are disregarded in analysis.
- The temperature variation during an adiabatic charging of a capacitor is larger than the change in temperature during its adiabatic discharging. The fulfillment of this condition is ensured by the position of the working point, which is chosen on the decreasing segment of function $d\varepsilon/dT(T)$ in the region of the negative extremum of the dependence shown in Fig. 1b. Then, the known relation [5] for the adiabatic EC effect

$$\Delta T_{ad} = \int \frac{T}{C_E}\left(\frac{\partial}{\partial T}\varepsilon(T)\right)EdE = \int \frac{T}{C_E}\gamma(T)EdE,$$

leads to the validity of the assumption under which the heat capacity C_E of an EC element for a given electric field strength has the form [5]

$$C_E = C_0 + E^2 T\frac{\partial^2 \varepsilon}{\partial T^2} \tag{1}$$

In this equation, C_0 is the heat capacity of the capacitor disregarding the action of the electric field.

- The capacitors whose temperature varies periodically in time exchange heat regeneratively via a heat conductor. For this reason, we assume that this element of the cooling line is a regenerator with temperature T_R. A similar assumption is used in thermodynamic analysis of the Stirling and Ericson regenerative cycles.

Let us consider the sequence of processes in a ferroelectric cooling structure taking into account the above assumptions. We will analyze the change in the volume-averaged temperature of the capacitors upon make-and-break of electric field in a steady-state regime. In this case, transient processes can be ignored, and we can assume that the temperature of each capacitor deviates from its steady-state value only as a result of external action. Consequently, the ferroelectric in the steady state performs a thermodynamic cycle consisting of three processes (isothermal, adiabatic, and heat exchange at constant voltage). These processes are shown in Fig. 2, where point *C* lies above point 2 and point 3 lies below point *B*. The former point (2) is located higher due to assumption (i_v), while the latter point (3) lies lower since the difference in the temperature levels of the two elements in the stationary state is smaller than the electrocaloric temperature effect.

The first ("Cold") element performs the *A–B–C* cycle, while the second ("Hot") element performs the 1–2–3 cycle; the processes occur with a time shift determined from the thermal constant of the capacitors. The difference between these elements is that the "Cold" element is discharged isothermally with absorption of heat and is charged adiabatically upon heating, while the "Hot"

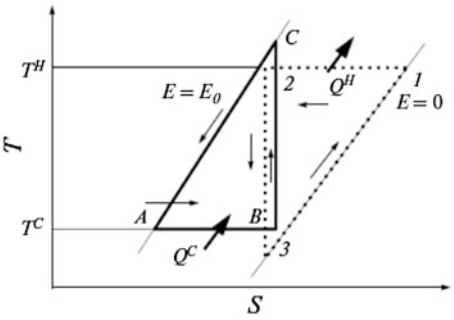

Fig. 2 The thermodynamic switching cycle for EC elements in a solid state line. "Cold" element performs on *A–B–C* cycle, while "Hot" element follows on *1–2–3* cycle

element is charged isothermally with heat release and is discharged adiabatically upon cooling. The above assumptions form the basis of thermodynamic analysis and estimation of the cooling efficiency and refrigeration efficiency Ψ for processes of switching in the solid-state line. Let us consider the cyclic sequence of processes in the cooling system under the above assumptions.

During isothermal discharging in contact with thermal conductors (*A–B*), the "Cold" EC element absorbs heat. The amount of heat *QC* defined, according to [42], as

$$Q_C = T_A\left(\frac{\partial\varepsilon(T_A)}{\partial T}\right)_E E^2 \tag{2}$$

is removed from the object being cooled at temperature TC = TA (the temperature corresponding to point A. The "Hot" element is heated from temperature T_3^H to T_B^C during the period following the discharge (at the initial segment of process 3–1). In the course of process B–C, adiabatic charging of the "Cold" element takes place, and its temperature increases from to $T_C^C > T^H$. In process 3–1, the "Hot" element continues to receive heat at constant electric field strength and is heated from T^H to $T_1^H = T_2^H = T^H$. At the next instant, the ED "Cold" element is charged at temperature $T_C^C = T^H$. The regenerator temperature has a mean value $T_R < T^H$. In process 2–3, the "Hot" element is discharged adiabatically, and its temperature decreases from T_2^H to T_3^H. As a result, a temperature differences appears at the ends of the regenerator, and a heat flow directed from the "Cold" to "Hot" element appears in the regenerator due to thermal conductivity of the material.

In process *C–A*, the "Cold" capacitor is cooled in a constant electric field from temperature T_B^C to $T_A^C = T_C$ due to the temperature gradient. In process 1–2, the "Hot" capacitor is discharged isothermally; therefore, the heat Q_H released to the ambient is given by

$$Q_H = T_H\left(\frac{\partial\varepsilon(T_H)}{\partial T}\right)_E E^2 \tag{3}$$

Amount of heat Q_H is greater than Q_C; the temperature at one end of the regenerator is T^H and at the other end, $T_B^C > T^H$; consequently, a heat flow from the "Cold" to "Hot" element appears in the regenerator. Then, the cycle is repeated.

The possibility of processes *C–A* and 2–3 is determined by the following factors: over a short time interval, the regenerator receives amount of heat Q_{REG} from one side and loses heat Q''_{REG} at the other side; after a certain time, the system must come to thermal equilibrium characterized by zero temperature gradients. However, in the process considered here, a temperature gradient due to the difference in the boundary conditions of the "Hot" and "Cold" elements always exists. Processes *C–A* and 3–1 were considered while solving the thermal conductivity problem, in which the regenerator is treated as a heat-conducting rod with initial temperature *TR* under periodic action of local sources with a phase shift and

asymmetric boundary conditions [36]. It follows from the solution to this problem that temperature at the middle of the regenerator in the steady-state regime is constant, and temperature oscillations occur at its ends with a certain time shift. Consequently, the regenerator whose temperature has decreased due to cooling during the adiabatic discharging of the "Hot" element completely absorbs the heat supplied to the regenerator during heating as a result of adiabatic discharging of the "Cold" element and returns to the initial temperature in accordance with the above assumptions. The removed energy is $Q = C_E(T_3^H - T_A^C)$.This process takes place because the 1–2–3 cycle leads the *A–B–C* cycle. Consequently, the relation between the heat capacity and thermal conductivity of the regenerator determines the lower temperature level (T_C).

Thermodynamic analysis of the physical processes is carried out as a rule by one of the following two methods: method of cycles (circular processes) or thermodynamic potential method. Let us determine the refrigeration efficiency of the cooling structure under investigation using the method of thermodynamic cycles. In accordance with this method of analysis, we must find the amount of thermal energy received by the ferroelectric at a low temperature and the amount of thermal energy given away by the ferroelectric at a high temperature. The difference in these energies is the work of the cycle, and the ratio of the heat received by the ferroelectric to the work is the efficiency of a given thermodynamic cycle (refrigeration efficiency). The absolute thermodynamic efficiency of a thermal cycle is defined as the ratio of the refrigeration efficiency to the refrigeration efficiency of the Carnot cycle.

For each capacitor, heat can be supplied or removed in the course of isothermal discharging or charging or as a result of rapid adiabatic change in temperature. Let us denote the adiabatic change in the temperature of the "Cold" element by ΔT_{ad}^C and the change in the temperature during adiabatic cooling of the "Hot" element by ΔT_{ad}^H. Then, the amounts of heat ΔQ_1^H and ΔQ_2^H supplied to and removed from the "Hot" element are

$$\Delta Q_1^H = C_0^H(T_1^H - T_3^H),$$
$$\Delta Q_2^H = \Delta Q_H = T_H\left(\frac{\partial \varepsilon(T_H)}{\partial T}\right)_E E^2.$$

The work L_H of the cycle performed by the "Hot" element is $L^H = \Delta Q_2^H - \Delta Q_1^H$. The amount of heat ΔQ_1^C and ΔQ_2^C supplied to and removed from the "Cold" element are

$$\Delta Q_1^C = C_E^C(T_C^C - T_A^C),$$
$$\Delta Q_2^C = \Delta Q_C = T_A\left(\frac{\partial \varepsilon(T_A)}{\partial T}\right)_E E^2.$$

Work L^C of the cycle performed by the "Cold" element is $L^C = \Delta Q_2^C - \Delta Q_1^C$. The total work L_Σ of the entire cycle is the sum of these works:

$$L_\Sigma = L^C + L^H = \Delta Q_2^C - \Delta Q_1^H = \Delta Q_C - \Delta Q_H.$$

This result was obtained from the condition of complete heat exchange in the regenerator:

$$\Delta Q_1^H = \Delta Q_1^C,\ C_0^H(T_1^H - T_3^H) = C_E^C(T_C^C - T_A^C)$$

using the above equation, we obtain the following equality:

$$C_0^H \Delta T_{ad}^H = C_E^C \Delta T_{ad}^C.$$

This equality holds in spite of the fact that $\Delta T_{ad}^C < \Delta T_{ad}^H$ since the heat capacity of the ferroelectric depends on the electric field and $C_E^C > C_0^H$. Heating of the "Hot" element occurs is zero electric field, while cooling of the "Cold" element occurs in field E. The heat capacity can be calculated from the expression

$$C_E^C = C_0(T_C) + E^2 T_C \frac{\partial^2 \varepsilon(T_C)}{\partial T^2}.$$

Let us find the refrigeration efficiency Ψ:

$$\Psi = \frac{\Delta Q_C}{L_\Sigma} = \frac{\Delta Q_C}{\Delta Q_H - \Delta Q_C},$$

where energy ΔQ is calculated for the isothermal EC effect:

$$\Delta Q = \int T\left(\frac{\partial}{\partial T}\varepsilon(T)\right) EdE = \int T\gamma(T)EdE \approx T\gamma(T)E^2$$

Eliminating E_2, we obtain the following expression for the refrigeration efficiency:

$$\Psi = \frac{T_C\gamma(T_C)}{T_H\gamma(T_H) - T_C\gamma(T_C)}.$$

The version of the expansion of the temperature dependence of the derivative of permittivity $\gamma(T) = d\varepsilon/dT(T)$ for barium titanate (see Fig. 1) is a power series including the numerical coefficient up to T^4:

$$\gamma(T) = a + bT + cT^2 + dT^3 - gT^4.$$

The values of these coefficients are chosen by approximating the curve representing the function $\gamma(T)$ using the least square method. This approximation leads to numerical coefficients of the series and the values of the thermodynamic efficiency for EC-line

$$\eta_t = \frac{\Psi}{\Psi_{Carnot}},\ \Psi_{Carnot} = \frac{T_C}{T_H - T_C},$$

where Ψ_{Carnot}—refrigeration efficiency of the Carnot cycle.

At a temperature of 272.5 K of the "Cold" capacitor and the value of $\Delta T = 0.5$ K, the cooling efficiency is 0.57, where ΔT is the range of temperature variation over a switching cycle ($T_H - T_C$). At a temperature 271.5 K and $\Delta T = 0.5$ K, the cooling efficiency is 0.1.

If we assume that $\Delta T = 2$ K and the temperature of the "Cold" capacitor is 271.5 K, the efficiency is 0.6.

Thermodynamic analysis of the cooling process in the solid-state line shows that the maximal value of the efficiency of solid-state coolant is attained for temperatures close to the negative extremum on the temperature dependence of the derivative of permittivity. The thermodynamic efficiency of the EC converter is estimated. Under the assumption that the range of temperature variation in a thermodynamic cycle is $\Delta T = 2$ K and the temperature of the "Cold" BST capacitor is 271.6 K, the efficiency amounts to 0.6 Carnot. This value considerably exceeds the efficiency of vapor-compression refrigerating energy converters.

To attain cooling in a wide temperature range, it is expedient to use cascade systems. In this case, the solid-state cooling line is an element of a refrigerating cascade connecting the object to be cooled and the heat sink (heat exchanger). To elevate the efficiency of a cascade cooling structure, the EC elements are prepared from materials with the Curie temperature (and point of inflection) increasing from element to element. From the standpoint of thermodynamic efficiency, the search for materials with a large thermal EC effect is not the most vital trend in development and designing of solid-state cooling structure. In our opinion, the choice materials with a gently sloping γ(T) dependence in the region of extremum of this function and the possibility to vary the critical temperature of the ferroelectric in a wide range are more important. Solid solutions of ferroelectrics (e.g., BST perovskite and relaxant materials such as PMN–PT), in which the critical temperature can be controlled in a wide temperature range by varying their composition, satisfy these requirements best of all.

2.2 Temperature Drop by Parametric Effect

The principal difference between solid-state cooling and the gas refrigerator is that for the thermo-mechanical systems, the frequency of the gas pressure variation is in the range (0.1–1) Hz. From over hand for the EC cooling rate of the electric field variation frequency is limited only by the relaxation time of polarization. In addition, the polarization depends not only on the electric field, but also from mechanical stress, pressure, etc. Parametric change electrocaloric factor may lead to a substantial increase in the EC effect. In this case the quasi-static approximation is not valid, so you must use a dynamic model.

Consider the EC effect expression, written in terms of polarization P

$$C_E dT = -T\frac{\partial P}{\partial T}dE,\ dT = -\frac{T}{C_E}\frac{\partial P}{\partial T}dE \tag{4}$$

where T is the absolute temperature, P is the polarization, E is the electric field strength, CE is the heat capacity at a constant field strength, and γ is the EC coefficient

$$\gamma_{ec} = -\frac{T}{C_E}\frac{\partial P}{\partial T}.$$

It follows from Eq. (4) that the maximum change in the temperature takes place in a region of maximum pyroelectric coefficient $p = \partial P/\partial T$. For ferroelectrics, this is a region of temperatures close to the Curie point TC, where the Landau–Ginzburg theory of second-order phase transitions is applicable. According to this theory, the polarization as a function of the field strength can be expressed as follows:

$$E = aP + bP^3, \tag{5}$$

where $a = a_0(T - T\mathrm{C})$, a_0 is the Curie–Weiss constant, and b is the coefficient of nonlinearity. A maximum change in the temperature upon a single application or removal of the field, $\Delta T = 40$ K, was observed for a 450-nm-thick $Pb_{0.88}La_{0.08}Zr_{0.65}Ti_{0.35}O_3$ film at a field strength of 1,250 kW/cm. It should be noted that a comparison of the two sides in the formula (4) for the available experimental data shows that the right side is 10–15 % larger than the left side [1, 32]. This fact has been recently explained in [46]. Determination of polarization P is based on the measurement of a hysteresis curve during cyclic variation of the field strength. In this case, it is necessary to take into account the dynamic effects and replace relation (5) by the Landau–Khalatnikov equation:

$$r\frac{\partial P}{\partial \tau} = E - aP - bP^3 \tag{6}$$

where r is the effective "internal" resistance. For small r, the polarization can be expressed as follows [47]:

$$P = P_{st} + P_{dyn}, P_{dyn} = -\frac{r}{a + 3bP_{st}^2}\frac{\partial P_{st}}{\partial t} \tag{7}$$

where P_{st} is the quasi-static polarization determined from Eq. (5) and P_{dyn} is the dynamic correction that accounts for an increase in ΔT in the case of indirect measurements. The adiabatic equation in the Landau–Ginzburg theory is written as follows [55]:

$$T - T_0 = \frac{a_0}{\kappa}(P^2 - P_0^2) \tag{8}$$

where κ is a constant quantity and T_0 and $P_0$are the initial temperature and polarization, respectively. The validity of Eq. (8) has been repeatedly confirmed (see e.g., [1, 23, 25, 32, 55]. Thus, Eq. (5) is applicable to the description of quasi-static processes, while the dynamic processes should be describes using Eq. (6).

In the immediate vicinity of the Curie point, the left-hand side of this equation should be additionally refined by adding terms describing the pyroelectric and piezoelectric currents [47].

The problem encountered in creating cooling structure is the organization of a thermodynamic cycle. Under the adiabatic conditions, the overall change of the temperature upon the application and removal of electric field is zero. Therefore, it is necessary to implement non-adiabatic processes (isothermal, or those with constant E or P). The adiabaticity can be violated, e.g., by using thermal switches or taking into account heat exchange with the environment and the inhomogeneity of the temperature field in a sample [20, 21, 51, 52]. For example, the results of numerical calculations for $BaSrTiO_3$ (BST) [20, 21] showed that, after 1,000 switching cycles, the system attains a steady-state regime, in which the temperature oscillates about the average value that is 20 K below the initial temperature. The measurements of temperature during periodic variation of the electric field were performed by Wiseman [55]. In the first cycle, the application of the electric field led to an increase in the sample temperature by 0.043 K, while switching the field off led to a decrease in the temperature by 0.046 K, so that the total temperature change per cycle was $\delta T = 0.003$ K. This dependence has been qualitatively predicted by Lawless [23]. The EC effect can be amplified by using multilayer structures. In particular, it was shown in [10] that at switching frequency of 1 Hz in BST ceramics the EC effect is increased on 2.5 K by introducing second layer of EC material.

In the present investigation, we have used the dependence of polarization P on an auxiliary parameter, which can be represented by a magnetic field (magnetoelectric effect) or a mechanical stress. Let us consider the free energy functional of the following type:

$$F = F_0(T) + \frac{aP^2}{2} + \frac{bP^4}{4} - EP + \alpha\eta P^2 + \frac{\beta\eta^2}{2} - \eta\sigma \tag{9}$$

where $F_0(T)$ is a certain function of the temperature, η is the second (in addition to P) order parameter, σ is an external field, and α and β are constant coefficients. In what follows, η implies deformation and σ denotes elastic stress, so that β is the elastic modulus and α is the piezoelectric modulus. Note that, for crystals, α, β, η, and σ are tensor quantities [12]. The free energy given by expression (9) describes a piezoelectric effect that is quadratic with respect to polarization P. Writing the condition of minimum for the free energy according to equation (9) yields the following system of equations:

$$(2\alpha\eta + a)P + bP^3 = E,\ \alpha P^2 + \beta\eta = \sigma \tag{10}$$

from which the order parameters P and η are determined as functions of the known variables E and σ. For $\alpha = 0$, the second equation of system (10) describes the usual Hooke's law. Excluding η from this equation, we obtain the following relation:

$$(2\frac{\alpha}{\beta}\sigma + a)P + (b - \frac{2\alpha^2}{\beta})P^3 = E \tag{11}$$

which determines the dependence of polarization P on E, η, and σ. The entropy and heat capacity of the system are determined as follows:

$$S = -\frac{\partial F}{\partial T},\ C_E = -T(\frac{\partial^2 F}{\partial T})_E.$$

Having denoted$F_0''(T) = k$ we obtain the following expression for the EC coefficient:

$$\gamma(T, \sigma) = \frac{pP(T, \sigma)}{k + a_0 pP(T, \sigma)} \tag{12}$$

According to the above formulas the EC coefficient γ depends on stress σ. According to the results of calculations [38], the EC effect in compressed (clamped) BST ceramics is characterized by $\gamma_{cl} \approx 0.6\gamma_{free}$, where γ_{cl} and γ_{free} are the EC coefficients for the clamped and free ceramics. For $BaTiO_3$, the analogous relation is $\gamma_{cl} \approx 0.8\gamma_{free}$ [1]. It is important to note that the process of external field variation can be isothermal (with neglect of the barocaloric effect), which makes it possible to organize the most effective thermodynamic cycle, a four-stage Carnot cycle. First, the electric field is applied to a preliminarily clamped sample, and the sample is adiabatically heated. At the next stage, the external pressure is isothermally reduced to zero. At the third stage, the electric field is switched off. Finally, the sample is isothermally clamped. The resulting change δT in the sample temperature per cycle can be exactly calculated using formulas (4), (8), and (11). It can also be qualitatively estimated through ΔT. Adopting the ratio of $\gamma_{cl}/\gamma_{free} = 0.8$, we obtain $\delta T = 0.2\Delta T$, which significantly exceeds the corresponding value in the absence of a control mechanical stress. Indeed, $\delta T = (0.01 - 0.02)\Delta T$ according to numerical calculations [10, 20, 35] and $\delta T = 0.05\Delta T$ according to experimental data [55].

Since the organization of a Carnot cycle is technically difficult, let us consider a simpler case of periodically varying applied electric field and mechanical stresses:

$$E = E_0 \sin(\omega t),\ \sigma = \sigma \sin(\omega t + \varphi),$$

where E_0 and σ_0 are the amplitudes, ω is the frequency, and φ is the phase shift. In this case, the EC coefficient can be expressed as follows:

$$\gamma \approx \gamma_0(1 + \gamma \sin(\omega t + \varphi)) \tag{13}$$

where γ_0, γ_1, and φ are constant (time-independent) parameters. The results of a numerical solution of (4) and (13) for a lead magnesium niobate–lead titanate (PMN–PT) ceramics are presented in the Fig. 3. As can be seen, a difference between the initial and steady-state temperatures strongly depends on the phase shift, and both heating and cooling of the ceramic sample can take place. Thus, by

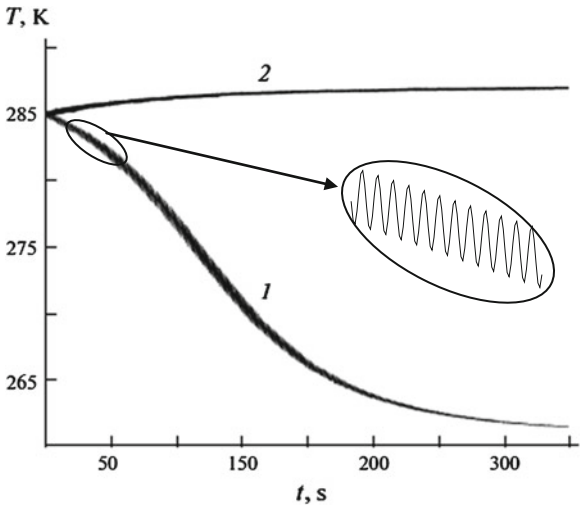

Fig. 3 The time variation of the temperature of PMN–PT ceramics in response to periodic oscillations of the applied electric field and mechanical stress with a relative phase shift of (*1*) $\varphi = \pi$ and (*2*) $\varphi = 0$

consistently varying the electric field and external pressure, it is possible to ensure a five- to ten- fold increase in the EC effect. The same approach can be used to enhance the magnetocaloric effect. It was demonstrated [49] that a 1 GPa pressure applied to $La_{0.69}Ca_{0.31}MnO_3$ single crystals increases the phase transition temperature by 25 K, thus decreasing the magnetocaloric effect to less than half.

Finally, it should be noted that there are different variants in selecting the order parameter η and external force σ. In piezomagnetics, it is possible to develop pressure by applying a magnetic field. The pressure can also be produced using the second layer of a piezoelectric, to which voltage E_2 is applied consistently with E. Another possible variant employs the barocaloric effect controlled by the electric field. In addition, it is possible to use multiferroics, in which the caloric effect not only depends on the main parameters (temperature and field strength), but can also be modulated by some other parameter.

From the presented analysis suggests that the use of nonlinear dynamic effects can produce a significant increase in the cooling effect. A more accurate calculation can be made only if we know the dynamic characteristics of the ferroelectric.

3 Dynamic Characteristics of Electrocaloric Materials

3.1 Dynamic Polarization in Electrocaloric Materials

Differences in the experimental approaches, measurement techniques, and objects used in this study hinder the realistic assessment of possibilities of the EC effect application in solid-state cooling devices. In this context, a topical problem is developing a theoretical approach to description of the EC response in ferroelectric

material excited by periodic variations of the external electric field. This process results in permanent dynamical change of thermodynamic parameters and a temperature inside the EC-cooling structure. More adequate model of EC-based cooling structure could be built just due to physical processes dynamics study.

Traditionally just static model is considered and it does not take into account any dynamic effects. The EC effect in a sample is described by the following classical formula:

$$\Delta T = -T \int_{E_1}^{E_2} \frac{1}{\rho C_E} \frac{dP}{dT} dE = -T \int_{E_1}^{E_2} \frac{\gamma_{ec}}{\rho} dE \tag{14}$$

where ΔT is the sample temperature variation relative to its initial value T, C_E is the heat capacity of the given material at a constant electric field strength, ρ is the material density, $P = P(T, E)$ is the polarization, and E_I and E_2 are the initial and final field strengths, respectively.

Formula (14) is derived in an adiabatic approximation and provides quite accurate description of the EC effect during quasi-static variation of the electric field E [24]. If the sample is involved in heat exchange with the surrounding medium, the temperature distribution becomes inhomogeneous and equation (14) has to be replaced by a more complicated expression [20, 26, 36, 45] that takes into account thermal relaxation processes in the EC element.

This chapter presents the results of an investigation of the influence of a polarization relaxation on the EC effect in a periodically varying electric field. The characteristic relaxation time is assumed to be small compared to the period of oscillations of the electric field.

A dynamic equation relating the electric field E and polarization P in a ferroelectric material was written by Landau and Khalatnikov (Landau et al. [22]) in the following form:

$$\alpha \frac{dP}{dt} = E(t) - aP - bP^3 \tag{15}$$

where $a = a_0(T - T_0)$; α, a_0, and b are constant coefficients; and T_C is the Curie temperature. From the standpoint of physics, a change in the sample polarization is equivalent to the presence of a current $J = \partial P/\partial t$ that, in turn, leads to the appearance of a dynamic field $E_\mathrm{Dyn} = \alpha J$, where α is the effective internal resistance. In what follows, the electric field is assumed to vary with the time according to a harmonic function as $E(t) = E_0 \sin(\omega t)$, where E_0 is the field amplitude and ω is the circular frequency.

Introducing the characteristic relaxation time $t_\mathrm{R} = \alpha/|a|$ and a parameter $s = \omega t\mathrm{R}$, which is assumed to be small ($s \ll 1$), Eq. (15) can be rewritten in the following form:

$$s \frac{dy}{dx} = -\sin(a)y - y^3 + e_0 \sin(x) \tag{16}$$

where $y = \sqrt{\frac{b}{|a|}}P$, $e_0 = \frac{E_0}{|a|}\sqrt{\frac{b}{|a|}}$, $x = \omega t$, are dimensionless quantities. Let us seek a solution to Eq. (16) for a stationary regime, in which case the initial conditions are insignificant [30] and represent this solution in the form of a series in powers of the small parameter s as follows:

$$y = \sum_{n=0}^{\infty} y_n(x)s^n \tag{17}$$

Substituting expression (17) into Eq. (16) and equating coefficients at the same powers of s, we obtain a recurrent set of equations for determining coefficients $y_n(x)$. The first equation that corresponds to the terms not containing s has the following form:

$$\sin(a)y_0 + y_0^3 - e_0\sin(x) = 0 \tag{18}$$

which coincides with the stationary Landau–Ginzburg equation. For y_0 at $T < T_C$, we can select any stable root of the three ones for Eq. (16) or the single root of this equation for $T > T_C$.

From the next equation, which is obtained for the terms involving s, we obtain the following coefficient at the first-order term in series (17):

$$y_1 = -\frac{y_0'}{\mathrm{sgn}(a) + 3y_0^2}.$$

The high order terms with $n > 1$ in series (17) are also readily determined from the subsequent recurrent equations. Restricting the consideration to the first two terms in series (17), we obtain the following approximate formula for the polarization:

$$P(t) \approx P_0(t) + P_1(t) \tag{19}$$

where P_0 is the quasi-static polarization determined from the Landau–Ginzburg equation and P_1 is the dynamic correction to P_0. This correction has the following form:

$$P_1(t) = -\frac{\omega\alpha E_0\cos(\omega t)}{(a + 3bP_0^2)^2} \tag{20}$$

It should be noted that formulas (19) and (20) remain valid in the vicinity of the Curie point, but they are inapplicable at the switching point where $P_0^2 = -a/(3b)$.

These formulas are readily generalized to the case of an arbitrary dependence of polarization P on the field E, which corresponds to the following equation:

$$s\frac{dP}{dt} = F(P, E(t), t) \tag{21}$$

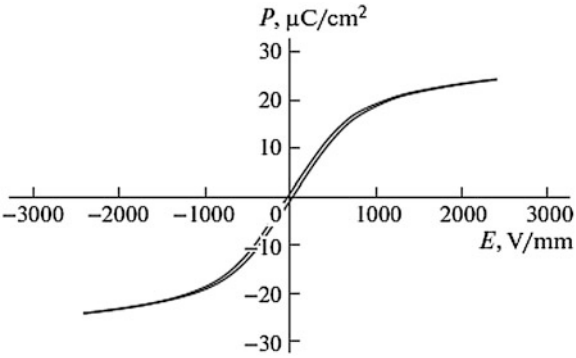

Fig. 4 The polarization hysteresis observed for a paraelectric phase of $Pb(Mg_{1/3}Nb_{2/3})O_3$–$PbTiO_3$ ceramics [12]

Here, $F(P, E(t), t)$ is an arbitrary function, in particular, polynomial of a higher power than that in Eq. (15). The asymptotic behavior of a solution to Eq. (21) in a stationary regime is described by the following expression:

$$P(t) = P_0(t) + s\frac{P_0'}{\frac{\partial F(P,E(t),t)}{\partial P}} + O(s^2) \tag{22}$$

An analysis of the obtained results leads to the following conclusions. First, formulas (19) and (20) can be used to describe the hysteresis in a paraelectric phase (i.e., at $T > T_C$), in which case Eq. (18) has a single solution. According to this, the hysteresis (Fig. 4) observed in experiments [16] is readily explained by correction (20). Indeed, for $E(t) \sim \sin(x)$, this correction can take two values that correspond to the different signs of $\cos(x)$ and lead to the two branches (hysteresis) in the $P(E)$ plot. Using the reported experimental data [16], it is possible to determine the relaxation parameter α for the given ferroelectric material. Denoting the values of polarization at $(E = 0)$ by P_U and $P_D (P_U > P_D)$, we obtain $P_0|E = 0 = 0$ and

$$\alpha = \frac{a(P_U - P_D)}{2\omega E_0}.$$

Second, the presence of correction (20) leads to additional dependence of the dielectric permittivity on the frequency.

Third, we can define the dynamic spontaneous polarization of a ferroelectric material as $P_{SDyn} = P(E = 0)$, that is, as the value of polarization at the intercept of the $P(E)$ curve with the P axis. Then, formula (20) yields the relation

$$P_{SDyn} - P_s = \frac{\alpha\omega E_0}{a^2},$$

where P_S is the static spontaneous polarization. The latter is $P_S = \sqrt{-a/b}$ for $a < 0$, $T < T_C$ and $P_S = 0$ for $T > T_C$. Thus, the dynamic spontaneous polarization is always greater than the static one. In the particular case of a paraelectric

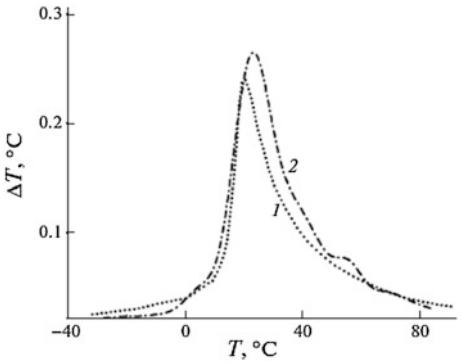

Fig. 5 The temperature dependence of the EC response (*1*)—measured for $Pb(Mg_{1/3}Nb_{2/3})O_3$–$PbTiO_3$ ceramics (Hagberg et al. [16]) and (*2*)—calculated using the temperature dependence of the spontaneous polarization

phase with $P_S = 0$, there exists a dynamic polarization P_{SDyn} that is caused by the periodic variation of the electric field.

Fourth, since formula (14) for the EC effect is obtained in the quasi-static approximation, it involves the static polarization P_0. Therefore, replacing P_0 by the dynamic polarization $P_1 = P_{Dyn}$ in Eq. (14) (as it was done in [29]) leads to an overstated magnitude of the EC effect, whereby the maximum EC response shifts toward higher temperatures. This fact was established in Neese et al. [33], where the difference between the results of calculations (using P) and the data of measurements varied within 15–20 % depending on the temperature.

Figure 5 shows the typical temperature dependence of the E_C response ΔT measured for $Pb(Mg_{1/3}Nb_{2/3})O_3$–$PbTiO_3$ ceramics (curve 1) [16], in comparison to the results of the calculations using the temperature dependence of the spontaneous polarization.

In conclusion, the proposed theoretical approach based on the Landau–Khalatnikov model shows that adequate description of the EC effect for a ferroelectric material in an alternating electric field is provided by E_q. (19) with the temperature-dependent polarization. We believe that the use of a quasi-static model in this case is incorrect and leads to erroneous results.

3.2 Thermal Hysteresis in Ferroelectrics Capacitance

Thermodynamics processes in cooling structure, presented in Sect. 1, along with adiabatic temperature change process, include, as well heating (cooling) process for element under permanent field. This process is accompanied with polarization changing. That is why it is important to know polarization dependence on temperature under heating and cooling modes. It defines specific of operational cooling system prototype based on multilayer structure. Study of thermal hysteresis in layered structures provides necessary data for comparative analysis of various materials applied to cooling structure.

This section presents the results of cooling time regime influence, electric field and electrical conductivity influence on temperature hysteresis of the capacitor structures based on $Ba_xSr_{1-x}TiO_3$ (BST) and $Pb(Mg_{1/3}Nb_{2/3})O_3$–$PbTiO_3$ (PMN-PT) ceramics. The BST ceramics is very common ferroelectric ceramics type for various electronics application [24, 44, 53], however it has rather high level of dielectric losses ($\tan\delta \sim 10^{-2}$) for microwave [53] and temperature control by means of electrocaloric effect applications. Another disadvantage of BST ceramics is not reproducible properties after initial action of electric field (dielectric hysteresis) [13, 53]. An introduction of Mg or Mn dopants [7, 56, 57] allows effectively managing by electric properties of BST ceramics. The better results ($\tan\delta \sim 10^{-3}$) at sufficiently high level of control (dielectric permittivity dependence on electric field) have been achieved using Mg doping [6, 8, 19]. However, the doping of BST ceramics does not give a possibility fixing dielectric hysteresis and satisfying to the requirements for temperature control components using electrocaloric effect [6, 8, 34, 45, 47]. Thus, the study of temperature and electric field influence on dielectric properties of ferroelectric ceramics of two types (BST and relaxor PMN–PT) is perspective and necessary.

Temperature dependences of the capacitance and dielectric losses of ferroelectric ceramics were measured at frequency 1 MHz. It is known that BST solid solutions has no the dispersion of dielectric permittivity (ε) in a range of frequencies $f = (10^2$ to $10^{12})$ Hz. We carried out the frequency measurements of dielectric permittivity and quality factor [34] of BST:Mg investigated ceramic samples in a range (10^3 to $5{\cdot}10^{10}$) Hz that have confirmed an absence of frequency dispersion ε and a little reduction of the quality factor (increase of dielectric losses) with frequency enhancement.

Temperature dependences measurements of the capacitance and dielectric losses were carried out at frequency 1 MHz using automatic impedance digital bridge device E7-12 [34]. The measurement error did not exceed 0.02 pF and the fractional error of dielectric permittivity definition was no more than 0.2 %. The amplitude of a measuring field was stabilized at 2.5 V/cm. The leakage current measurements of sample conductivity were carried out by means of electrometer B7-30 in a range of 10^{-13} to 10^{-5} A. The fractional error of current measurement did not exceed 10 %.

Voltage capacitance characteristics (VCC), current–voltage characteristics (CVC) and temperature dependencies $C(T)$ were measured at various values of bias voltage. The installation was capable of performing measurements for values of bias voltage in the range $U = \pm 1{,}000$ V. During the measurements process the temperature was automatically controlled. The absolute error of temperature measurements did not exceed 0.05 K in the temperature range 78–400 K, temperature variation rate was changed in the range (0.025–0.5) K/s. The temperature cycle of differential capacitance measurements consisted of the cooling process from 290 K down to 140 K and further heating process back to 290 K. The dependencies of differential capacitance on temperature $C(T)$ were measured for ten values of bias voltage—from 0 to 900 V.

Applicability of the ferroelectric material for technical purposes is determined by the values of dielectric permittivity ε, dielectric losses tanδ and tunability coefficient (k). The coefficient is the ratio of the brought dielectric permittivity at zero electrical field to ε value at maximal intensity of electrical field. The Mg additives to BST compound decrease dielectric losses, that it is important for microwave applications. The investigated samples of $Ba_xSr_{1-x}TiO_3$ ($x = 0.55$) have contained 12 wt.% of Mg additive. Latter we will consider this dependence on the dielectric loss tangent of the concentration. The selected BST compound has dielectric losses parameter tan $\delta = (5.5–6.0)\cdot10^{-3}$ that is much lower comparing with original BST compound. Earlier [34] we have shown than the magnesium additive decrease dielectric permittivity, at Mg concentration of (10–25) wt.% dielectric permittivity is standing at the level $\varepsilon = (500–600)$ and the tunability coefficient is sufficiently high that is important as for microwave tunable devices as well as for thermal conversion processes. Thus, the indicated Mg additive concentration corresponds to the required working parameters of the capacitor structures $\varepsilon \geq 500$; tan $\delta \leq 10^{-2}$ and in microwave region $k \geq 1.2$ at the fields $E_{max} = 4–5$ V/μm.

The composition and weight content of Mg additives, the synthesis temperature (1,350–1,540) °C have been chosen to provide a weak interaction between two main phases in ferroelectric ceramic. The porosity of the ceramic samples did not exceed 5 %. The polished ceramic samples having disk shape with the thickness 0.5 mm and diameter 5–6 mm were covered by gold electrodes using magnetron sputtering. The X-ray diffraction analysis has shown that the samples have contained of perovskite cubic phase and the second Mg_2TiO_4 spinel phase. It was found that basic BST perovskite phase has contained magnesium atoms (up to 5 at.%) that change the parameter of a crystal lattice.

The $0.87Pb(Mg_{1/3}Nb_{1/3})O_3$—$0.13PbTiO_3$ (PMN–PT) ceramic samples were sintered using the technology described earlier [16] in the laboratory of microelectronics and material physics of the University of Oulu. The ceramics thickness was 1–1.4 mm and the electrode diameter—7.6 mm. The X-ray diffraction analysis has showed a presence of single perovskite phase.

Temperature measurement cycle for the differential capacitance was based on samples cooling from 290 K down to 140 K and heating back up to 290 K. Differential capacitance dependence of temperature $C(T)$ was measured for ten values (from 0 to 900 V) of the bias voltage at the rate of temperature change of 0,025 K/s. Figure 6 shows the $C(T)$ dependencies for BST sample at absence of electrical field and two values of bias voltage from the indicated region. The dielectric permittivity for the chosen samples had the following maximal values $\varepsilon_m(0) = 6{,}700$, $\varepsilon_m(300\text{ V}) = 4{,}150$, $\varepsilon_m(900\text{ V}) = 1{,}900$. An increase of bias voltage leads to capacitance value decrease; the temperature of C_m is displaced to the right on temperature axis. Such temperature displacement of $C(E, T)$ dependencies is usual for the ferroelectric materials with wide and spread phase transition of the second order [24, 44]. However on dependences of temperature hysteresis both in ferroelectric and in paraelectric phase was observed.

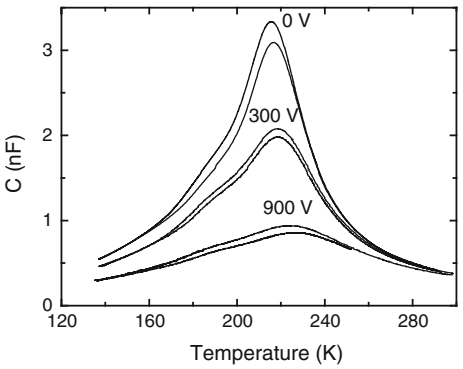

Fig. 6 The temperature dependence of BST ceramics sample capacitance at temperature variation rate 0.025 K/s and several bias voltage values

As a temperature hysteresis we understand not only a displacement of temperature maximum of the sample capacitance at cooling (T_{m1}) and heating (T_{m2}) – ($\Delta T_m = |T_{m1} - T_{m2}|$), but also relative reduction of the maximum values of capacitance at cooling (C_{m1}) and heating

$$(C_{m2}) - (\Delta C_m / C_{m1}) = (C_{m1} - C_{m2}) / C_{m1}.$$

The temperature of capacitance hysteresis of the investigated BST:Mg samples has showed unusual behavior of perovskite material at influence of external electric field. The nonlinearity reduction in most part of perovskite materials show that hysteresis phenomena become less appreciable, i.e. the hysteresis is decreased at influence of electric field $E \sim 10^5$ V/m [44, 53] In our case in the beginning the temperature hysteresis of the ceramic capacitance was decreased at voltage influence, and, from the voltage ~500 V that corresponds E ~ 10^5 V/m, the hysteresis was increased.

The increase of cooling-heating process rate leads to the enhancement of temperature hysteresis. This effect is illustrated in Fig. 7, where temperature dependence of capacitance is presented at zero bias voltage and temperature variation rate 0.5 K/s. It is necessary to notice that the temperature hysteresis was

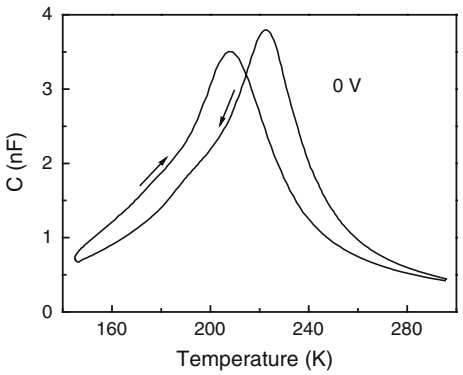

Fig. 7 The temperature hysteresis of BST ceramics sample capacitance at temperature variation rate 0.5 K/s

depended on a speed of cooling and heating of the samples. So the temperature hysteresis in absence of voltage at speed of temperature change ~0.025 K/s has made $\Delta T_m = 2$ K and the maximum of the capacitance temperature dependence at heating of the samples was displaced to higher temperature. The temperature hysteresis for the same sample at temperature variation rate ~0.5 K/s is increased to $\Delta T_m = 27$ K (Fig. 7). Thus a displacement direction to a maximum of temperature dependence T_{m2} is changed on opposite, the temperature hysteresis of the capacitance $\Delta C_m/C_{m1}$ is also increased. The heating mode has appeared more sensitive to a speed of temperature change, than a cooling mode. It has been established that at speed of change of temperature $V \sim 0.05$ K/s the temperature hysteresis ceases to depend on a speed of cooling of the samples [16]. The increase of cooling-heating process rate leads to the enhancement of temperature hysteresis. This effect is shown in Fig. 7. The dependence of temperature hysteresis on temperature variation rate $\Delta T_m(v)$ has a linear character.

The temperature hysteresis in BST:Mg structures was measured in more details and voltage capacitance characteristics were obtained at 300 K (Fig. 8). The capacitance indeterminacy on VCC reached several per cent and it was observed at every value of voltage. Such VCC plot corresponds to the hysteresis loops of large width that is typical behavior for relaxor ferroelectrics. In ferroelectric phase the hysteresis reaches the tens of per cents. At $T = 300$ K and zero bias voltage the permittivity value $\varepsilon(0) = 830$.

Dielectric loss factor at zero bias voltage is $\tan\delta \sim 10^{-4}$ and most part of the samples has demonstrated $\tan\delta$ increase with bias voltage enhancement. Fig. 9 illustrates sharp decrease of $\tan\delta$ at Mg doping additive increase in the region 0–60 wt.% to BST compound. However, from practical point of view the increase of Mg additive higher than 20 wt.% is not appropriate because of considerable decrease of capacitance control factor.

The conductivity of the samples and existence of free charge carriers can render a significant influence on the hysteresis phenomenon [6], therefore the measurements of current–voltage characteristics are helpful. Typical voltage-capacitance and current–voltage characteristics of BST ferroelectric ceramics with Mg additives is presented in Figs. 10 and 11. Figure 11 shows three regions of CVC in

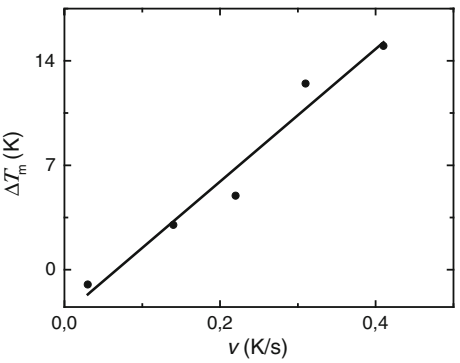

Fig. 8 The shift in temperature hysteresis dependence on temperature variation rate

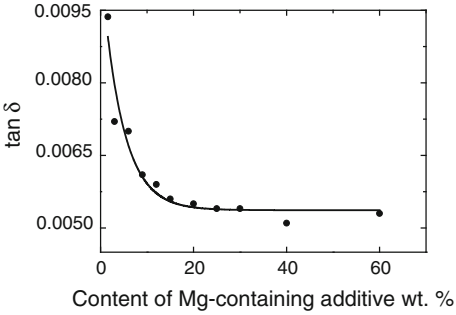

Fig. 9 The dependence of the dielectric losses on the contents of Mg-containing additives ($f = 10$ GHz)

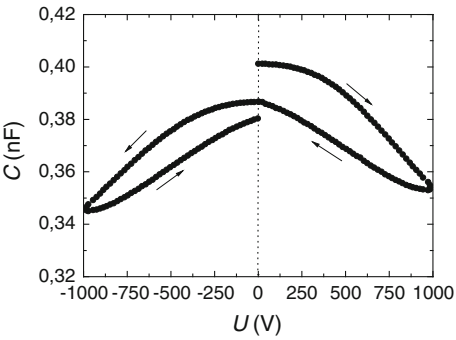

Fig. 10 The capacitance–voltage characteristics of BST based sample

double logarithmic scale. At low voltage the dependence corresponds to Ohm's law. At the following region, where current decrease is observed, a voltage increase is revealed, so some kind of negative differential resistance is identified. At higher voltage (more than 500 V) exponential current growth is exhibited. Estimation of sample resistance for the Ohm-related region results with $R \sim 6 \times 10^{10}\ \Omega$, the specific samples resistivity was found to be $(3.2 \pm 0.4) \times 10^{-10}$. $\Omega^{-1}\text{m}^{-1}$. Earlier we showed in [6] that the presence of negatives differential resistance and exponential growth on CVC is currently leading to high value of hysteresis value.

An observation of same characteristics for PMN–PT ceramics gives the temperature dependencies of the capacitance at zero and two other values of bias voltage, as it is shown in Fig. 12. An increase of bias voltage leads to a lowering of $C(T)$ curves and temperature of the capacitance maximum is shifted insignificantly ($\Delta T_\text{m} = \pm 1$ K). Dielectric hysteresis on $C(U)$ dependences is not observed, as it is shown in Fig. 13. The Ohm's law region and negative differential resistance regions are distinguished clearly, but exponential growth at higher voltages is not found (Fig. 14). The following values of dielectric characteristics for PMN–PT samples was calculated by the experimental results: $\varepsilon_\text{m}(0) = 18{,}000$, $\varepsilon_\text{m}(450) = 16{,}000$, $\varepsilon_\text{m}\ (950) = 12{,}000$. At T = 300 K the dielectric permittivity was 8,200; tan $\delta \sim 10^{-1}$, $R = 2 \times 10^{-10}\ \Omega$.

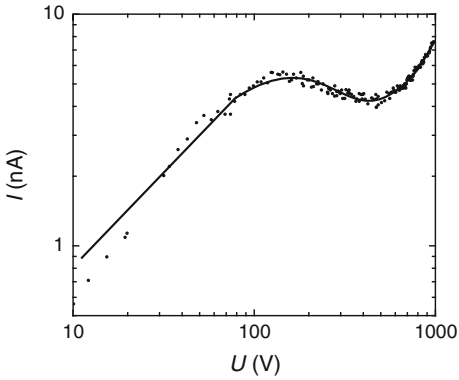

Fig. 11 The current–voltage characteristics of BST based sample

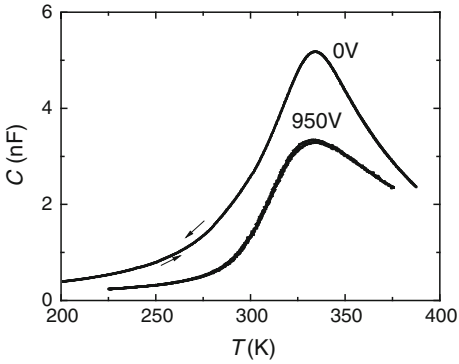

Fig. 12 The temperature dependence of PMN–PT sample capacitance for the several values of bias voltage

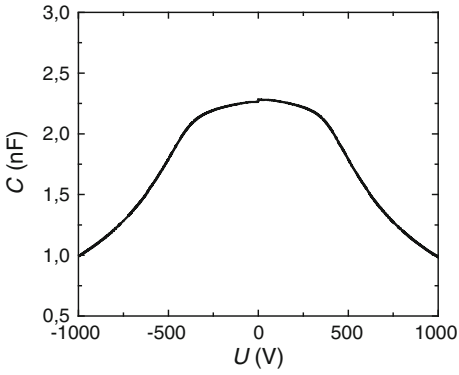

Fig. 13 The capacitance–voltage characteristics of PMN–PT sample

The investigations of voltage capacitance and current voltage characteristics (Figs. 11 and 14) and the dependencies $C(T)$ have shown that the phenomenon of temperature hysteresis exhibited in BST ceramic with Mg-content additives could be explained by means of high level of inhomogeneities, which are contained in

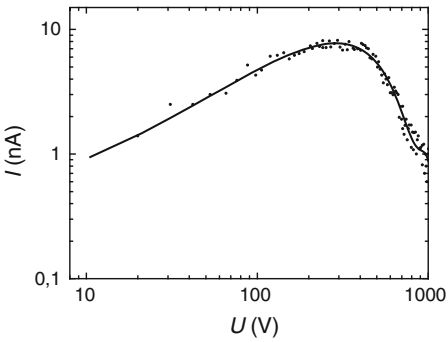

Fig. 14 The current–voltage characteristics of PMN–PT sample

the ceramic samples in comparison to significantly higher homogeneous single-phase PMN–PT ceramics. Scanning electron microscope (SEM) images of BST ferroelectric ceramics containing Mg additives were obtained using the JSM-6460LV JEOL microscope. One of these images is presented in Fig. 15. The BST ceramics contain the crystallites and noncrystalline inclusions of various dimensions (1 … 10 μm). Apparently the ceramics contain at least two phases: main perovskite phase and intergranular contaminations (shown as B and I in Fig. 15). Intergranular medium also contains small crystallites of (0.3 … 5) μm.

The X-ray microstructural analysis have shown that basic BST phase is composed of two perovskite phases with lattice parameters (3.935–3.941) Å and (3.954–3.966) Å. Pure BST ceramics of the chosen composition has lattice parameter of 3.9513 Å. The first phase, which has lower than pure BST ceramics lattice parameter, is related to the phase with lower content of Ba ions. It is known [48, 53] that in some solid solutions of BST the lattice parameter decreases linearly from 4.040 Å (at x = 1) to 3.905 (at x = 0). Slight increase of lattice parameter of the second phase can be associated with partial substitution of Ti^{4+} in BST [18, 19] lattice with Mg^{2+}, or with increase of Ba content up to $x \sim 0.6$ (reference value

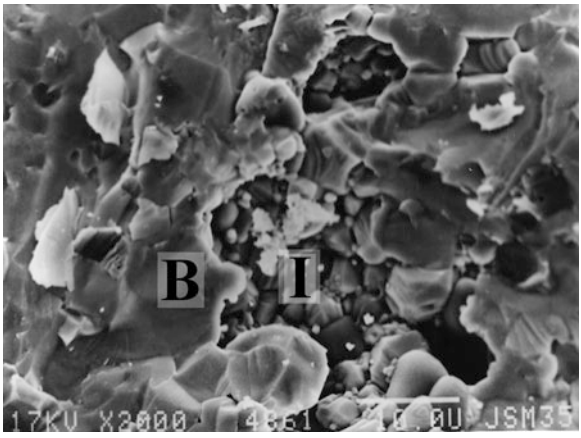

Fig. 15 The scanning electron microscope image of the surface of ferroelectric BST ceramic with magnesium additive

for $x = 0.6$ equals to 3.965 Å). Thus composite BST ceramics with magnesium additives has hetero-phase structure, composed of basic BST phase solid solution and phase with magnesium content. Some ceramics areas composing 1–30 % of the crystalline magnesium containing phase render considerable influence on highly defective phase of ferroelectric ceramics.

The shown micro-inhomogeneities lead to temperature hysteresis, and it could be connected with the following purposes:

- An enhancement of mechanical strains and deformations and following relaxation of the mechanical stress in the process of sequential cooling and heating cycles.
- An appearance of the defects internal electrical fields at the inhomogeneities borders that decrease dielectric permittivity at the region of the fields presence.
- Screening of the free carriers of the polarized regions of the crystals.

The appearance and relaxation of the mechanical strains, i.e. existence of elastic hysteresis mechanism is supported with the fact that temperature hysteresis value depends on sample cooling and heating rate (Figs. 6, 7 and 12).

Existence of internal electric fields of the defects in perovskite ferroelectrics is supported with the dependence of capacitance temperature hysteresis on applied field, and it relates to existence of dielectric hysteresis at all values of bias voltage (Fig. 6). Dielectric hysteresis of capacitance was discussed earlier, [7, 54] and the estimation of internal electric field values was given $E \sim (5 \times 10^5$ to $10^6)$ V/m.

Apparent influence on dielectric [6, 34] and consequently temperature hysteresis is exerted by conductivity of samples. Temperature hysteresis of the ferroelectric capacitance is decreased in the range, where current decreases—the range of negative differential resistance,—and it increases as voltage values, which corresponds to exponential growth of current ($E \sim 2{\cdot}10^5$ V/m). Free charge carriers, screening polarized areas in the single crystals, which do not take part in further processes of repolarization. This is the third cause of temperature hysteresis. This mechanism should have most influence in ferroelectric phase. Second and third causes of temperature hysteresis reveal the mutual influence to each other.

So we have obtained the temperature hysteresis of the capacitance basing on the ceramics $Ba_{0.55}Sr_{0,45}TiO_3$ containing 12 wt.% of Mg complex additive. There is the correlation between temperature hysteresis and the thermocycling regime of the measurement process. The increase of thermocycling process leads to the growth of temperature hysteresis. The high limit rate of temperature variation was 0.05 K/s. Exponential growth of the current at voltage intensity $2{\cdot}10^5$ V/m caused an essential influence on the temperature hysteresis. The phenomenon of temperature hysteresis is connected with high level of the micro inhomogeneities with Mg-containing doping.

3.3 Thermo-Relaxation Time in Electrocaloric Materials

One of the trends in studies is the measurement of temperature variations occurring under the action of an electric field. The temperature effect is measured using direct and indirect methods. The most widely used indirect method is based on the Maxwell relations

$$(dD/dT)_E = (dP/dT)_E = (dS/dT)_T,$$

where S is the entropy, E is the electric field strength, D is the electric induction, P is the polarization, $D = \varepsilon_0 E + P$, ΔT is the adiabatic change in temperature, ΔS the isothermal change in entropy for a material of density ρ, heat capacity C_E, and for electric field variation from E_1 to E_2. The Maxwell relations lead to [7]

$$\Delta S = -\int_{E_1}^{E_2} \left(\frac{dP}{dT}\right)_E dE.$$

Considering the complex nature of ferroelectric relaxor materials, the actual temperature response can not be determined exactly by calculating the temperature effect on the basis of these formulas, and the dynamics of the response cannot be analyzed.

In recent years, the temperature effect has been measured directly with an electric bias voltage applied to ferroelectric capacitors. It was shown that the change in temperature due to the electrocaloric effect (which was obtained by recalculating the temperature dependence of spontaneous polarization) and direct temperature measurements give noticeably different results [46]. On the one hand, this can be explained by not quite correct employment of the quasi-static model for the recalculation. On the other hand, standard measuring facilities introduce distortions comparable with the value of the effect being measured and are characterized by a considerable inertia which is inadmissible for rapidly occurring processes. For example, the heat capacity of a microthermocouple is commensurate with the heat capacity of a ferroelectric film in which the electrocaloric effect is measured.

In this study, we propose a new method for measuring rapid changes in temperature, which is based on the use of a ferromagnetic film resonator as a temperature gauge.

The saturation magnetization M_0 of a ferromagnetic demonstrates a strong temperature dependence [37], which can be used for temperature measurements. Figure 16 shows the $M_0(T)$ curve for an yttrium–iron garnet (YIG) epitaxial film. It is important that in the range of room temperatures (200–400 K), this curve can be approximated by a linear dependence of the type $M_0(T)$ [G] $= 4532 - 9.3\,T$.

Consequently, the resonance frequency of the microwave ferromagnetic film resonator is also a function of temperature, which can form the basis of the precision method for studying rapid variations in temperature.

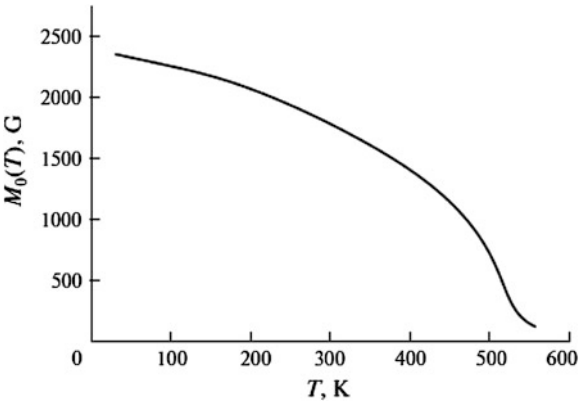

Fig. 16 The temperature dependence of the saturation magnetization for yttrium–iron garnet

Let us drive the expression for the temperature dependence of the resonance frequency of a microwave ferromagnetic film resonator. The dispersion equation for spin waves existing in the ferromagnetic medium can be written in the form [56]

$$\omega^2(kL) = [\omega_H + \omega_M - \omega_M P(kL)] \times [\omega_H + \omega_M P(kL)\sin^2\varphi] \tag{23}$$

where ω and k are the frequency and wavenumber of a spin wave; $P(kL) = 1 - [1 - \exp(-kL)]$, L being the thickness of the ferromagnetic film; ϕ is the angle between the direction of propagation of the wave and magnetic displacement vector H_0, $\omega_H = \mu_0\gamma H_0$, $\omega_M(T) = \mu_0\gamma M_0(T)$, γ being the gyromagnetic ratio, and $M_0(T)$ being the temperature dependence of the saturation magnetization. The eigenfrequencies of the resonator can be obtained from Eq. (23). The wavenumbers for the resonator eigenmodes are quantized as follows:

$$k = k_{gr} = \pi\sqrt{\left(\frac{q}{a}\right)^2 + \left(\frac{r}{b}\right)^2} \tag{24}$$

where a and b are the linear sizes of a thin-film resonator with $L \ll a$ and b, and q and r are the integers determining the multiplicity of the resonance. Proceeding from simple geometrical considerations, we can write angle ϕ in the form

$$\sin^2\varphi = \left(\frac{q/a}{k_{gr}}\right)^2 \tag{25}$$

Figure 17 shows the temperature dependence of the main resonance frequency of a ferromagnetic film resonator magnetized in the plane of the film. Symbols show experimental results and the solid line corresponds to the theoretical calculations based on the linear approximation of the temperature dependence of saturation magnetization.

Differentiating the temperature dependence of the resonance frequency, we can show that the sensitivity of the temperature measurement by the proposed method

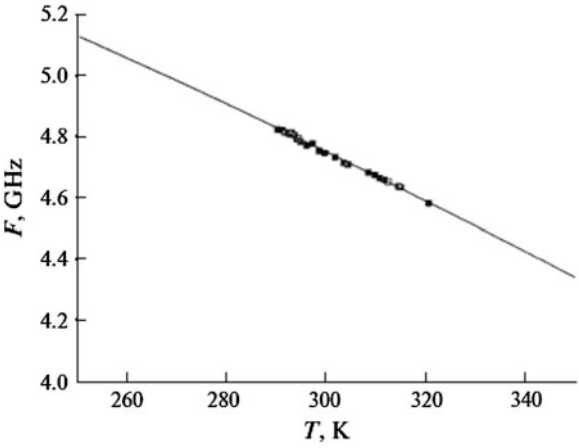

Fig. 17 The temperature dependence of the main resonance frequency of the ferromagnetic film resonator

is 10^{-4} K/kHz. Modern measuring instruments make it possible to measure the frequency in the range of interest up to several kilohertz. To analyze the dynamics of the electrocaloric effect, we used in our experiments a parallel-plate $Pb(Mg_{1/3}Nb_{2/3})O_3$–$PbTiO_3$ (PMN–PT) ferroelectric ceramic capacitor. The Curie temperature of the 0.87PMN–0.13PT material was about 48 °C. The temperature dependences of the permittivity of the ferroelectric ceramic under investigation for different voltages across the capacitor are shown in Fig. 11. Figure 18 shows schematically the measuring circuit diagram. The tangentially magnetized ferromagnetic resonator is excited with the help of a short-circuited microstrip

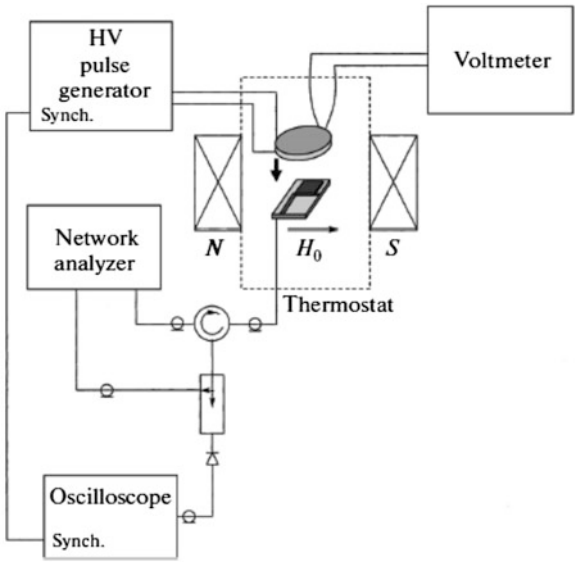

Fig. 18 The schematic diagram of the measuring unit

antenna. The resonator was cut from YIG epitaxial film 5 μm in thickness, which was grown on a 300-μm-thick gadolinium–gallium garnet substrate.

The resonator size in the plane was (2 × 2) mm^2. A ferroelectric capacitor with a high-voltage pulse generator connected to its plates is applied to the resonator on the side of the YIG film. The measuring prototype is placed into a thermostat, and its absolute temperature is measured by a constantan–manganin thermocouple. The external magnetic field in the measuring prototype region is produced by a samarium–cobalt magnet. The signal reflected from the measuring resonator is fed via a circulator to a directional coupler; a part of the signal is fed to the second port of the network analyzer, while the other part is fed to the detector of the oscilloscope synchronized with the high-voltage pulse generator. The resonance characteristic of the ferromagnetic resonator is registered by the network analyzer Rohde & Schwarz ZVA-40. The time variation of the temperature under the periodic action of the electric field (charging–discharging of the capacitor) is registered by the oscilloscope.

Recalculation of the temperature dependence of the resonant frequency shows that the sample is heated by 0.065 K and is cooled by 0.041 K relative to the temperature of the surrounding medium. Figure 19 shows oscillograms of the temperature response, which are plotted from the temperature shift of the ferromagnetic resonance frequency at the instant of the supply and removal of a high-voltage pulse. It can be seen that the time constant describing the temperature variation due to the electrocaloric effect amounts to 4.5 μs. A further change in temperature (cooling or heating) to the ambient level occurs over a period on the order of 10 μs, which is due to the thermal resistance between the sample and the thermostat. In this case, the fact that the Joule loss affects the shape of oscillograms must also be taken into account.

The experiments performed in the indicated temperature range have made it possible to construct the temperature dependence for the temperature response in the electrocaloric effect (Fig. 20).

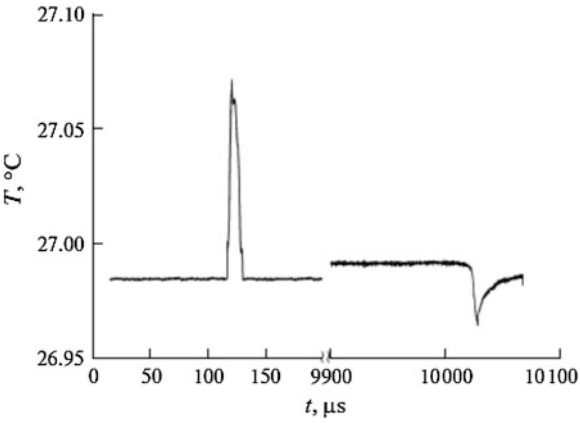

Fig. 19 The oscillograms of the temperature response for ferroelectric capacitor at instants of a high-voltage pulse applying and removing

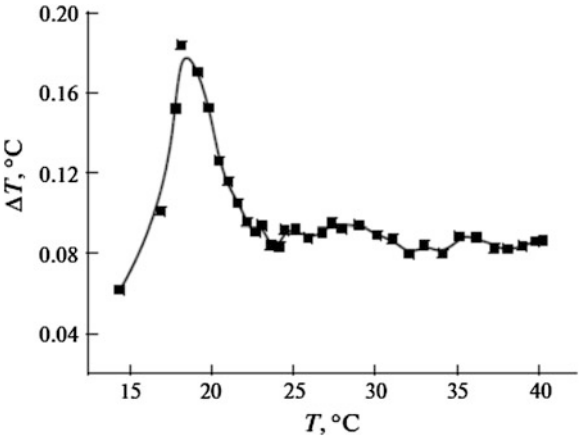

Fig. 20 The temperature dependence of the temperature response for electrocaloric effect in 0.87PMN–0.13PT ferroelectric capacitor

The curve shows that the peak of the electrocaloric effect lies in the range of 18 °C, which coincides with the peak of the derivative $d\mathrm{P}/dT$ this is in good agreement with thermodynamic relation (14).

4 Simulation of Electrocaloric Cooling Structure

4.1 Mathematical Model of Multicaloric Effect

One of the most promising approaches for practical realization of cooling device on the base of the ECE is a multilayered structure of ferroelectric, dielectric and metal alternating layers. The thicknesses of these layers as well as their thermal properties (e.g. thermal conduction and thermal capacity) must be chosen on the criterion of the cooling effect maximization. Moreover, in the case of a layered structure with layers differently distributed over temperature, temperature gradient and as a consequence heat flow take place. Therefore, in order to describe the thermal fields is necessary to use the heat equation not restricted by the simple model as described in Sect. 2. In addition, the presence of elastic stresses (caused by the boundaries of different materials, the thermal expansion of the layers, etc.) must be taken into account. For the purpose of the simultaneous description of electrical, thermal and elastic properties of the system we introduce the following quantities: vector of deformation u_i ($i = 1, 2, 3$), strain tensor

$$\varepsilon_{ij} = \left(u_{i,j} + u_{j,i}\right)/2$$

and stress tensor σ_{ij}. Here and below the symbol $\chi_{i,k}$ means $\partial\chi_i/\partial\chi_k$. Further we will use Einstein's notation for the summation of repeated indices.

The free energy density is given by:

$$F = (\bar{D}, \bar{P}, \varepsilon_{ij}, T) = F_0(T) + F_{Landau} + F_{elast} + F_{grad} + F_{coup} + F_{coup\ grad} \quad (26)$$

where $F_0(T)$ the independent on field part of the free energy. The Landau thermodynamic potential can be written in the form

$$F_{Landau} = \frac{a_i}{2} P_i^2 + \frac{a_{ij}}{4} P_i^2 P_j^2 + \frac{a_{ijk}}{6} P_i^2 P_j^2 P_k^2 - E_i P_i \quad (27)$$

which allows to describe the phase transitions of the first and second kind. Among the Ginzburg–Landau coefficients a_i, a_{ij}, a_{ijk} only the first one depends on the temperature: $a_i = a_{i0}(T - T_C)$, where a_{i0} is the Curie–Weiss constant. The elastic part of the free energy can be written as:

$$F_{elast} = C_{ijkl}\varepsilon_{ij}\varepsilon_{kl} + (T - -T_C)t_{ij}\varepsilon_{ij}. \quad (28)$$

Here C_{ijkl} is the elastic module tensor and t_{ij} is the thermal stress tensor [18]. The necessity of the second term introduction in the right part of (28) can be explained by the following fact. Even small change in temperature of layers with a small thickness results in significant temperature gradient (up to 10^6 K/m [18]). Note that the series expansion (28) is valid only in a small neighborhood of the Curie temperature where ECE is most powerful. The gradient terms can be represented as:

$$F_{grad} = \lambda_{ij} T_i T_j + g_{ijkl} D_{ij} D_{kl} \quad (29)$$

Here λ_{ij} is the thermal conductivity tensor, while g_{ijkl} are electrical gradient tensor coefficients. Let us mention that (29) includes the components of the electric displacement$\bar{D}$instead of polarization $\bar{P}$ (as performed in the standard approach [44]). This is because the presence of $(\nabla \bar{P})^2$ in (29) results in the continuity of the normal component of $\bar{P}$ at the interface, which is in contravention of Maxwell's equations. Piezoelectric part of the free energy can be expressed by the formula [40]:

$$F_{coup} = e_{ijk}\varepsilon_{ij}P_k + e_{ijkl}\varepsilon_{ij}P_k P_l. \quad (30)$$

Here e_{ijk} is the piezoelectric constants tensor and e_{ijkl} are modules of the electrostriction. The first term in (30) describes the piezoelectric effect, which exists under certain restrictions on the symmetry of the ferroelectric material. The second term is responsible for the electrostriction. In the last summand of the free energy we collect the terms which describe the influence on the polarization and temperature (as well as strain gradients of these quantities)

$$\begin{aligned} F_{coup\ grad} =& b_{ij}P_i T_{,j} + b_{ijk}\varepsilon_{ij}T_{,j} + f_{ijk}(T - T_C)\varepsilon_{ij,k} \\ &+ f_{ijkl}P_j\varepsilon_{jk,l} + d_{ijkl}\varepsilon_{ij}P_{k,l} + d_{ij}(T - T_C)P_{i,j}. \end{aligned} \quad (31)$$

There exist six possible variants of the pair-wise interaction for three variables $\bar{P}$, T, ε_{ij} and their gradients (the interaction with the gradient of any quantity of itself is not considered). In other words, the first pair of terms in (31) describes the

impact of ∇T on the polarization (i.e. thermopolarization effect or polarization thermogradient effect) and strain (i.e. elastic thermogradient effect). The second pair takes into account the impact of strain gradient on the temperature (flexothermal effect) and polarization (flexoelectric effect). The third pair is used to describe the polarization dependence on the gradient of temperature and deformation (thermal and elastic polarization gradient effects). The quantities b_{ij}, b_{ijk}, P_{ijk}, f_{ijkl}, d_{ij}, d_{ijkl} are the coefficients of the corresponding effects.

Further, the term $F_{coup\ grad}$ is possible to exclude from the consideration assuming the insignificance of described by this summand effects (some of them have not yet been found experimentally). However, in some cases these terms must be included, e.g. for the description of domain wall with high polarization and strain gradients.

Variation of (26) in the variables P, T, u_i gives:

$$E_i = a_i P_i + \frac{a_{ij}}{2} P_i P_j^2 + \frac{a_{ijk}}{3} P_i P_j^2 P_k^2 + e_{kli}\varepsilon_{kl} + e_{kjil}\varepsilon_{ij} P_l - g_{ijkl} D_{ij,kl} \tag{32}$$

It should be noted that there is no summation over i in (32).

$$\left(\lambda_{ij} T_j\right)_i - t_{ij}\varepsilon_{ij} = 0 \tag{33}$$

$$\sigma_{ij} = C_{ijkl}\varepsilon_{kl} + (T - T_C) t_{ij} + e_{ijk} P_k + e_{ijkl} P_k P_l. \tag{34}$$

Equations (32)–(34) should be supplemented by the standard boundary conditions at the interfaces:

$$T_1 = T_2,\ \lambda_{ij}^{(1)} T_{1,j} n_i = \lambda_{ij}^{(2)} T_{2,j} n_i,\ D_i^{(1)} n_i = D_i^{(2)} n_i,\ u_i^{(1)} = u_i^{(2)},\ \sigma_{ij}^{(1)} n_j = \sigma_{ij}^{(2)} n_j \tag{35}$$

which implies the continuity of temperature, heat flux, deformation vector, the normal component of electric displacement, and the stress tensor. The indices 1 and 2 in (35) indicate the value location with respect to number of considered media; n_i are components of the vector normal to the boundary. At the outer boundary it is possible to set temperature $T = T_0$, heat flow $\lambda_{ij} T_{,j} n_j = q_0$ or their linear combination $\lambda_{ij} T_{,j} n_j + H_0(T - T_0) = 0$. Here T_0 is ambient temperature, q_0 is heat flow on the boundary, H_0 is heat transfer coefficient.

The mechanical boundary conditions can consist of setting efforts $\sigma_{ij} n_{ij} = F_j$, displacement $u_i = u_{io}$, or have a mixed form. Here F_i, u_{io} are the components of forces and displacements at the boundary. The interface potential or the electrical intensity $E_i n_i = E_0$ can be used as electrical boundary conditions. Note that it is also possible to consider a combination of aforementioned quantities (impedance type boundary condition).

Let us now proceed to the dynamics of the processes. For the description of the polarization time dependence we use the equation of electrodynamics for non-equilibrium processes (the Landau-Khalatnikov equation)

$$r_i \frac{\partial P_i}{\partial t} = -\frac{\delta F}{\delta P_i},$$

that is

$$r_i \frac{\partial P_i}{\partial t} = E_i - g_{ijkl} D_{k,lj} - a_i P_i - \frac{a_{ij}}{2} P_i P_j^2 + \frac{a_{ijk}}{3} P_i P_j^2 P_k^2 - e_{kli} \varepsilon_{kl} + e_{kjil} \varepsilon_{ij} P_l \quad (36)$$

where r_i is phenomenological constants characterizing the relaxation time. Further, due to the lack of relaxation experimental data deformation component in (36) is considered in the static approximation. To describe the thermal processes we employ the Thompson equation

$$\partial Q = c\rho dT + T\left(\frac{\partial P_i}{\partial T} dE_i + \frac{\partial \varepsilon_{ij}}{\partial T} d\sigma_{ij}\right) \quad (37)$$

From (37) follows the equation of heat conduction

$$c\rho \frac{\partial T}{\partial t} = (\lambda_{ij} T_{,i})_j + Q(T, t, \varepsilon_{ij}, P) \quad (38)$$

where the quantity

$$Q = -T\left(\frac{\partial P_i}{\partial T}\frac{dE_i}{dt} + \frac{\partial \varepsilon_{ij}}{\partial T}\frac{d\sigma_{ij}}{dt}\right) - t_{ij}\varepsilon_{ij} \quad (39)$$

has the sense of the heat source.

The initial conditions for $t < 0$ have the form $T = T_0$, $P_i = P_{i0}$, $u_i = u_{i0}$, and must be self-consistently considered with (32)–(34). For a homogeneous medium the resulting equations are simplified. In this case, $\lambda_{ij} = \lambda\delta_{ij}$, $t_{ij} = t\delta_{ij}$, where $\delta_{ij} = 1$ for $i = j$ and $\delta_{ij} = 1$ for $i \neq j$ (λ is thermal conductivity and the coefficient t is proportional to the coefficient of the thermal expansion). In the next section we consider the equation (3.38) independently from (36) and (34).

4.2 Finite-Elements Simulation of Electrocaloric Cooling Structure

To create an experimental model of EC cooling structure appropriate to define the optimal ratio of the geometric dimensions, the magnitude of heat flux, frequency and pulse shape. This problem can be solved by the computer-based modeling.

At the first stage of modeling, for valuation calculations can be used simplified mathematical model of the electrocaloric cooling, which does not take into account the thermal stresses and thermal hysteresis of polarization.

As the working versions of the EC cooling structure we calculated using the finite element method a few version of cooling.

Let us consider a simple model of the cooling line shown in Fig. 21a. It consists of one electrocaloric element (ECE) separated from the environment by the heat conducting layers $[0 - x_1]$ and $[x_2 - L]$. We will investigate a one-dimensional

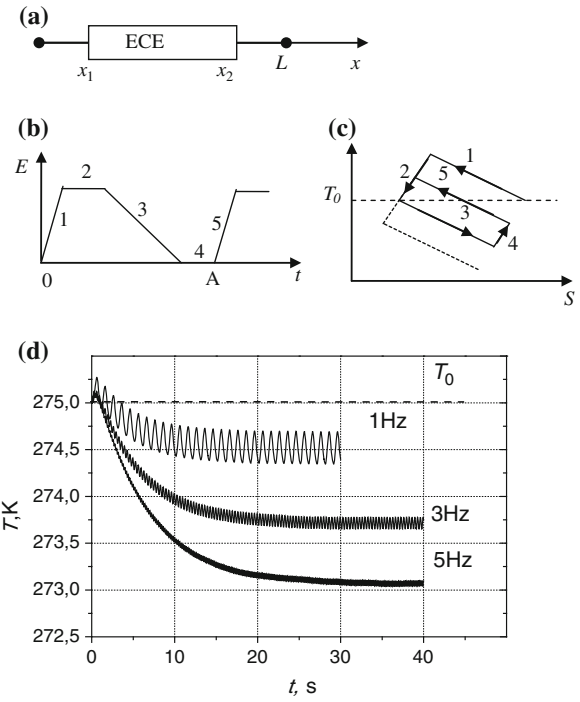

Fig. 21 The schematic diagram of a cooling line containing two ferroelectric capacitors **a**; temperature variation on the free end of the line (x = 0) upon antiphase harmonic switching of the capacitors **b**; thermodynamic cycle **c** in the element ECE; simulated time dependences of the cooling effect at various frequencies **d**

model under the assumption that the temperature changes affect only along the x axis. One boundary ($x = 0$) is thermally insulated, whereas the other boundary is held at a constant temperature T_0 equal to the initial temperature. The heat capacity $C(x)$ and thermal conductivity $\lambda(x)$ of the material are assumed to be constant within each segment of the line. In this case, the temperature distribution $T(x, t)$ along the line can be found by solving the heat conduction equation [18]

$$C(x)\frac{\partial T}{\partial x} = \frac{\partial}{\partial x}\lambda(x)\frac{\partial T}{\partial x} + Q(x,t,T) \tag{40}$$

which satisfies the initial and boundary conditions

$$T(x,0) = T_0;\ \ \lambda_0 \left.\frac{\partial T}{\partial x}\right|_{x=0} = 0,\ \ T|_{x=L} = T_0 \tag{41}$$

The function $Q(x, t, T)$ determines the quantity of heat released (or absorbed) by a thermal electrocaloric source and is expressed in the form given in [4, 20, 27]:

$$Q(x,t,T) = -T\frac{\partial P}{\partial T}\frac{dE}{dt} \tag{42}$$

where E is the electric field strength of the electrocaloric element and P is the polarization of the dielectric. The function $Q(x, t, T)$ is nonzero only within the

electrocaloric element. The time dependence of the electric field E has the period A and represents a function consisting of pulses shown in Fig. 21b. When a periodic sequence of pulses is supplied to the ferroelectric capacitor, the cycle shown in the T–S diagram (where T and S are the temperature and entropy of the element, respectively) (Fig. 21c) is executed, thus providing cooling of one of the ends of the electrocaloric element.

Interval 1 in Fig. 21 corresponds to charging of the capacitor and polarization of the ferroelectric, which leads to a decrease in the entropy. Within interval 2, the heat released during charging of the capacitor spreads over the structure, the capacitor remains charged, but its temperature is of the order of the initial temperature. Interval 3 corresponds to discharging of the capacitor, which leads to its cooling and an increase in the entropy due to depolarization. Within interval 4, the cooled capacitor is able to absorb the heat from the cooled body located at the point 0. The capacitor starts heating, and the next pulse 5 is supplied to prevent the capacitor from turning back to its initial state. Later on, the cycle is repeated (shown by the dotted line). Owing to the nonlinearity of the derivative of the polarization of the dielectric with respect to the temperature and the appropriate choice of the operating point, the quantity of the heat which the electrocaloric element can absorb during discharging exceeds the quantity of the heat released in the element during charging.

The numerical simulation of the cooling process was performed using the finite-element method.

The initial temperature was taken to be $T_0 = 275$ K, which was maintained at the end of the cooling line ($x = L$). The electric field amplitude was 5 V/μm. The ferroelectric capacitor and heat conducting elements were prepared from the $Ba_{0.6}Sr_{0.4}TiO_3$ (BST) ceramic material with the density $\rho = 6$ g/cm^3, the thermal conductivity $\lambda = 10$ W/(m K), and the heat capacity $c = 900$ J/(kg K).

Periodic pulses of the electric field were supplied to the electrocaloric elements with the frequency $f = 1/A$ ranging from 1 to 5 Hz. The pulses led to a periodic heating (cooling) of the electrocaloric elements and a redistribution of the temperature field along the structure. After a series of cycles in which the electric field was applied to the solid state structure, we determined the temperature distribution between the free end of the cooling line ($x = 0$) and the heat exchanger ($x = L$). Figure 21d presents the results of the computer simulation of the variation in the temperature. These results indicate that the temperature of the free end of the line substantially depends on the frequency of pulses. After a series of switching cycles, the system attains a steady state temperature regime and, then, the temperature oscillates only lightly around the average value.

A similar approach to the simulation of electrocaloric elements was used for a solid state line with two electrocaloric elements (see scheme in Fig. 22a). A heat conductor is located between two electrocaloric elements (ECE1, ECE2). The line contains two more heat conducting elements that connect the electrocaloric elements with the cooled object ($x = 0$) and the heat exchanger ($x = L$), respectively.

The results of the calculation of the thermal processes occurring in this structure are presented in Fig. 22b. When the additional element is used in the solid state

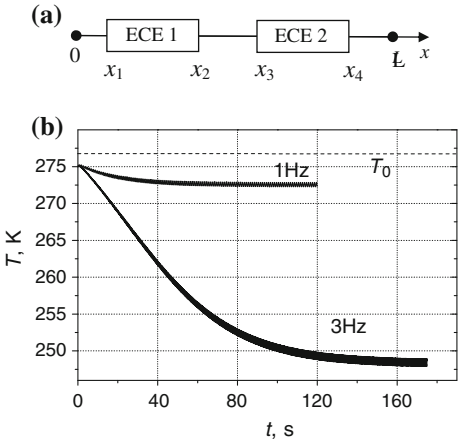

Fig. 22 The electrocaloric two-element line **a** and simulated time dependences of the cooling effect at various frequencies **b**

line, the gain in the temperature is equal to 2.5 K at a frequency of 1 Hz and reaches 25 K at a frequency of 3 Hz. In view of a large number of interrelated parameters of the structure under consideration (such as the lengths of elements and heat links, the phase shift, and the frequency of pulses), the optimum operating parameters of the line with two or more electrocaloric elements can be properly chosen only with the use of automated numerical analysis software and global optimization techniques.

The solid state cooling structure based on electrocaloric elements can have radial film geometry. In this work, we simulated a radial cooling structure based on a circular sapphire substrate with a thickness of 250 μm. A 1 μm thick BST film was deposited on the substrate. A circular double serrated electrodes cooling structure shown in Fig. 23a was formed on the surface of the BST film. A constant temperature was maintained at the outer boundary (periphery) of the radial microstructure. A series of periodic voltage pulses supplied to the electrode ring leads to the release or absorption of the thermal energy in the BST film. The use of ferroelectric films instead of ceramics allows one to substantially increase the repetition rate of switching pulses and, thus, to increase the heat flux power. The periodic temperature inhomogeneity is transferred into the substrate, which serves as a heat conductor. In the microstructure, there arises a heat flux directed along the radius of the structure. For particular physical and geometrical parameters of the microstructure, the heat flux is directed from the center to the periphery, which leads to the heat removal from the heated object placed at the center of the structure or to a decrease in the temperature.

In this work, we simulated a radial cooling structure with one line of electrodes. The diameter of the cooling structure was 0.4 mm, and the electrode gap width was 5 μm. The simulation was performed with the use of the finite element method at frequencies of 2.5 kHz and 10.0 kHz with applied field amplitude of 3 V/μm. Figure 23b presents the time dependences of the change in the temperature at the

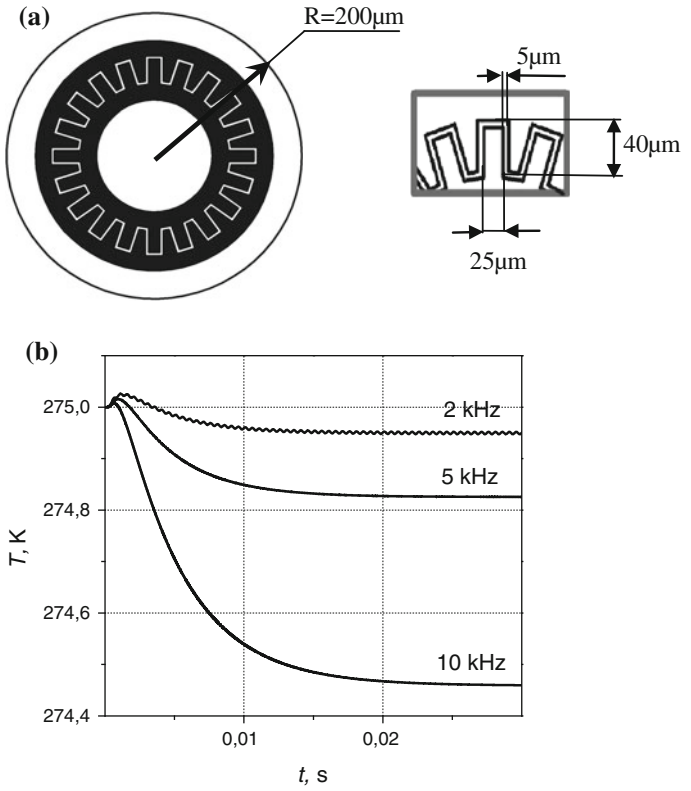

Fig. 23 The planar radial cooling structure prototype **a** and time dependences of the cooling effect in the structure center at various frequencies **b**

central point of the microstructure at different frequencies. The calculation has shown that, in the structure with one ring of electrodes, the decrease in the temperature can reach $\sim$0.5 K at a frequency of 10 kHz.

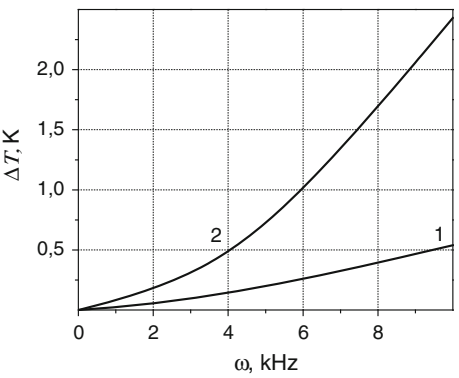

Fig. 24 The frequency dependences of the cooling effect for radial systems with one (curve *1*) and two (curve *2*) electrode lines

Figure 24 shows the frequency dependences of the cooling effect in the radial structure for systems with one (curve *1*) and two (curve *2*) electrode lines. As can be seen from this figure, the temperature difference across the radial cooling structure raises significantly with an increase in the number of serrated circular electrodes.

5 Conclusion

The theoretical and experimental results presented lead us to the conclusion that

- Sequence of several thermodynamic processes united into closed thermodynamic circle is the principle of operation for electrocaloric-based cooling structure. Therefore dynamic processes in ferroelectrics should be considered for adequate analysis of them.
- Criteria for selection and making materials for EC-based cooling structure include value of EC coefficient temperature derivative as well as EC coefficient value. EC-based cooling structure temperature operating point should be selected at maximum value of EC-index temperature derivative.
- Multilayer structure is the most rational solution for EC-based cooling structure. It provides specific heat raising and operational point temperature controlling.
- Cooling efficiency for EC-based cooling structure considerably depends on alternative electrical field frequency. The frequency is limited by EC-effect relaxation time being equal 1 μs. Heating and cooling velocity appreciably affects on thermal hysteresis value at permanent electrical field. Thermal hysteresis generation results in drop of EC-based cooling structure efficiency.
- Parametric effect provides considerable temperature drop in EC-based cooling structure. It could be reached by another caloric-effects (elastocaloric, magnetocaloric, barocaloric, etc.) materials introducing into ferroelectrics multilayer structure. Adjusted various exposure results in multicaloric effect within multilayer structure or EC-effect amplifying in ferroelectrics layers.
- Multilayer structures fabrication, investigation, thermal and physical characterisation should be considered as a perspective trend in electrocaloric-based cooling structure research.

Acknowledgments The Chapter preparing was supported by EU Grant No. 218282, ICPC Nanonet.

References

1. Akcay, G., Alpay, S.P., Matese, J.V., Rossetti, G.A.: Magnitude of the intrinsic electrocaloric effect in ferroelectric perovskite thin films at high electric fields. Appl. Phys. Lett. **90**(25), 252909 (2007)
2. Bazarov, I.P.: Thermodynamics. Pergamon Press, Oxford (1964)
3. Brodyanskii, V.M.: Autonomous Low_Power Criorefrigerators. Energoizdat, Moscow (1984). [in Russian]
4. Bulat, L.P.: Solid-state cooling systems. J. Thermoelectricity **3**, 15–21 (2007)
5. Camia, F.M.: Traite de Thermocinetique Impulsionelle Paris, Dunod (1967)
6. Dedyk, A.I., Kanareikin, A.D., Nenasheva, E.A., Pavlova, Y.V., Karmanenko, S.F.: *I-V* and *C-V* characteristics of ceramic materials based on barium strontium titanate. Tech. Phys. **51**(9), 59–64 (2006)
7. Dedyk, A.I., Karmanenko, S.F., Melkov, A.A., Pavlovskaya, M.V., Sakharov, V.I., Serenkov, I.T.: Influence of Mg and Mn doping on the RF-microwave dielectric properties of $Ba_xSr_{1-x}TiO_3$ films. Ferroelectrics **286**(1), 267–278 (2003)
8. Dedyk, A.I., Nenasheva, E.A., Kanareykin, A.D., Pavlova, JuV, Sinjukova, O.V., Karmanenko, S.F.: Tunability and leakage currents of (Ba, Sr)TiO3 ferroelectric ceramics with various additives. J. Electroceram. **17**(2–4), 433–437 (2006)
9. Epstein, R.I., Malloy, K.J.: Electrocaloric devices based on thin-film heat switches. J. Appl. Phys. **106**(6), 064509 (2009)
10. Es'kov, A.V., Karmanenko, S.F., Pakhomov, O.V., Starkov, A.S.: Simulation of a solid-state cooler with electrocaloric elements. Phys. Solid State **51**(8), 1574–1577 (2009)
11. Flerov, I.N., Mikhaleva, E.A.: Electrocaloric effect and anomalous conductivity of the ferroelectric NH_4HSO_4. Phys. Solid State **50**(3), 478–484 (2008)
12. Ginzburg, V.L.: Usp. Fiz. Nauk **38**(8), 490–525 (1949). (In Russian)
13. Golzman, B.M., Dedyk, A.I., Lemanov, V.V., Ter-Martyrosjan, L.T., Karmanenko, S.F.: Dielectric properties of planar structures based on ferroelectric Ba0.5Sr0.5TiO3.Pis'ma. Zh. Tekh. Fiz. **23**(32), 46–52 (1997)
14. Gurevich, A.G.: Ferrites at Super High Frequencies. Fizmatgiz, Moscow (1960). [in Russian]
15. Guyomar, D., Sebald, G., Guiffard, B., Seveyrat, L.: Ferroelectric electrocaloric conversion in $0.75(PbMg_{1/3}Nb_{2/3}O_3)$–$0.25(PbTiO_3)$ ceramics. J. Phys. D Appl. Phys. **39**(20), 4491 (2006)
16. Hagberg, J., Uusimaki, A., Jantunen, H.: Electrocaloric characteristics in reactive sintered $0.87Pb(Mg_{1/3}Nb_{2/3})O_3$–$0.13PbTiO_3$. Appl. Phys. Lett. **92**(13), 132909 (2008)
17. He, J., Chen, J., Zhou, Y., Wang, J.: Regenerative characteristics of electrocaloric Stirling or Ericsson refrigeration cycles. Energy Convers. Manage. **43**(17), 2319–2327 (2002)
18. Isachenko, V.P., Osipov, V.A., Sukomel, A.S.: Heat Transfer, p. 439. Energiya, Moscow (2001)
19. Karmanenko, S.F., Dedyk, A.I., Isakov, N.N., Gordeichuk, A.S., Semenov, A.A., Ter-Martirosyan, L.T., Hagberg, J.: Study of the effect of manganese impurities on dielectric characteristics of BSTO films. Tech. Phys. **41**(4), 498–502 (2001)
20. Karmanenko, S.F., Pakhomov, O.V., Prudan, A.M., Starkov, A.S., Es'kov, A.V.: Layered ceramic structure based on the electrocaloric elements working as a solid state cooling line. J Eur. Ceram. Soc. **27**(8–9), 3109–3112 (2007)
21. Khodayari, A., Mohammadi, S.: Solid-state cooling line based on the electrocaloric effect. IEEE Trans. Ultrason. Ferroelectr. Freq. Control **58**(3), 503–508 (2011)
22. Landau, L.D., Khalatnikov, I.M.: On the anomalous acoustical absorption near a second-order phase transition. Dokl. Akad. Nauk SSSR. **96**(3), 469–472 (1954)
23. Lawless, W.N.: Specific heat and electrocaloric properties of $KTaO_3$ at low temperatures. Phys. Rev. B. **16**(1), 433–439 (1977)
24. Lines, M., Glass, A.: Principles and Applications of Ferroelectrics and Related Materials. Clarendon Press, Oxford (1979)

25. Lu, S.G., Rožič, B., Zhang, Q.M., Kutnjak, Z., Li, X., Furman, E., Lee, G.J., Lin, M., Malič, B., Kosec, M., Blinc, R., Pirc, R.: Organic and inorganic relaxor ferroelectrics with giant electrocaloric effect. Appl. Phys. Lett. **97**(16), 162904 (2010)
26. Marvan, M., Jonscher, A.K., Fahnrich, J.: Electrocaloric effect as a cause of dielectric loss. J. Eur. Ceram. Soc. **21**(10–11), 1345–1348 (2001)
27. Mischenko, A.S., Mathur, N.D.: GB Patent #2420662 (2006)
28. Mischenko, A.S., Zhang, Q., Scott, J.F., Whatmore, R.W., Mathur, N.D.: Giant electrocaloric effect in the thin film relaxor ferroelectric $0.9PbMg_{1/3}Nb_{2/3}O_3$–$0.1PbTiO_3$ near room temperature. Appl. Phys. Lett. **89**(24), 242912 (2006)
29. Mischenko, A.S., Zhang, Q., Scott, J.F., Whatmore, R.W., Marhur, N.D.: Giant electrocaloric effect in thin-film $PbZr_{0.95}Ti_{0.05}O_3$. Science **311**(5765), 1270–1271 (2006)
30. Mishchenko, E.F., Rozov, NKh: Differential Equations with Small Parameter and Relaxation Oscillations. Nauka, Moscow (1975). [in Russian]
31. Morozovska, A.N., Eliseev, E.A., Svechnikov, G.S., Kalinin, S.V.: Pyroelectric response of ferroelectric nanoparticles: size effect and electric energy harvesting. http://arxiv.org/abs/0908.2311v1 (2009). Accessed 17 Aug 2009
32. Neese, B., Chu, B., Lu, S.G., Wang, Y., Furman, E., Zhang, Q.M.: Large electrocaloric effect in ferroelectric polymers near room temperature. Science **321**(5890), 821–823 (2008)
33. Neese, B., Lu, S.G., Chu, B., Zhang, Q.M.: Electrocaloric effect of the relaxor ferroelectric poly(vinylidene fluoride-trifluoroethylene-chlorofluoroethylene) terpolymer. Appl. Phys. Lett. **94**(4), 042910 (2009)
34. Nenasheva, E.A., Kanareikin, A.D., Dedyk, A.I., Pavlova, Y.V.: Electrically controlled BST-Mg ceramic components for applications in accelerator technology. Phys. Solid State **51**(8), 1557–1560 (2009)
35. Osipov, E.V.: Solid_State Cryogenics. Naukova Dumka, Kiev (1977). [in Russian]
36. Pakhomov, O.V., Starkov, A.S., Karmanenko, S.F., Es'kov, A.V.: Vestn. Mezhdunar. Akad. Kholoda. **2**, 31 (2007) [in Russian]
37. Pavlovskaja, M.V., Balakin, V.A., Dedyk, A.I., Karmanenko, S.F., Sakharov, V.I., Serenkov, I.T.: Influence of electron irradiation on the properties of ferroelectric $Ba_xSr_{1-x}TiO_3$ Films. Integ. Ferroelectr. **61**(1), 149–153 (2004)
38. Prosandeev, S., Ponomareva, I., Bellaiche, L.: Electrocaloric effect in bulk and low-dimensional ferroelectrics from first principles. Phys. Rev. B. **78**(5), 052103 (2008)
39. Radebaugh, R., Lawless, W.N., Siegwarth, J.D., Morrow, A.J.: Feasibility of electrocaloric refrigeration for the 4–15 K temperature range. Cryogenics **19**(4), 187–208 (1979)
40. Semenov, A.A., Karmanenko, S.F., Kalinikos, B.A., Srinivasan, G., Slavin, A.N., Mantese, J.V.: Dual-tunable hybrid wave ferrite-ferroelectric microwave resonator. Electron. Lett. **42**(11), 641–642 (2006)
41. Yu, S.V.: Analysis of the efficiency of an electrocaloric cryorefrigerator. Chem. Petrol. Eng. **31**(9), 501–506 (1995)
42. Sinyavskiy, YuV: Electrocaloric refrigerators: A promising alternative to current low-temperature apparatus. Chem. Pet. Eng. **31**(6), 295–306 (1995)
43. Sinyavsky, Y.V., Pashkov, N.D., Gorovoy, Y.M., Lugansky, G.E., Shebanov, L.: The optical ferroelectric ceramic as working body for electrocaloric refrigeration. Ferroelectrics **90**(1), 213–217 (1989)
44. Smolenskiy, A., Bokov, V.A., Isupov, V.A., Krainik, N.N., Pasinkov, R.E., Shur, N.S.: Ferroelectrics and antiferroelectrics. Nauka, Leningrad (1971)
45. Starkov, A.S., Karmanenko, S.F., Pakhomov, O.V., Es'kov, A.V., Semikin, D., Hagberg, J.: Electrocaloric response of a ferroelectric capacitor to a periodic electric field. Phys. Solid State **51**(7), 1510–1514 (2009)
46. Starkov, A.S., Pakhomov, O.V.: Influence of the dynamic polarization of a ferroelectric material on the magnitude of its electrocaloric response. Tech. Phys. Lett. **36**(1), 1–3 (2010)
47. Starkov, A.S., Pakhomov, O.V., Starkov, I.A.: Effect of thermal phenomena on a second-order phase transition in the Landau-Ginzburg model. JETP Lett. **91**(10), 507–511 (2010)

48. Su, B., Button, T.W.: Microstructure and dielectric properties of Mg-doped barium strontium titanate ceramics. J. Appl. Phys. **95**(3), 1382–1384 (2004)
49. Sun, Y., Kamarad, J., Arnold, Z., Zn, K., Chen, Z.: Tuning of magnetocaloric effect in a $La_{0.69}Ca_{0.31}MnO_3$ single crystal by pressure. Appl. Phys. Lett. **88**(10), 102505 (2006)
50. Sychev, V.V.: Complex THERMODYNAMIC SYSTEMS. Energoatomizdat, Moscow (1986). [in Russian]
51. Synyavsky, Y.V., Brodyansky, V.M.: Experimental testing of electrocaloric cooling with transparent ferroelectric ceramic as a working body. Ferroelectrics **131**, 321–325 (1992)
52. Tishin, A.M., Spichkin, Y.J.: The Magnetocaloric Effect and its Applications. IOP Publishing Ltd., Bristol, UK (2003)
53. Vendik, O.G.: Ferroelectrics at Microwaves. Sov. Radio, Moscow (1979)
54. Vendik, O.G., Dedyk, A.I., Dmitrieva, R.V., Zalonchkovskii, A.Y., Yu, L., Ruban, V.A.S.: Hysteresis of the permittivity of strontium titanate at 4.2 K. Sov. Phys. Solid State **26**(3), 412–415 (1984)
55. Wiseman, C.G.: Electrocaloric effect in potassium dihydrogen phosphate. IEEE Trans. Electron Devices **16**(6), 588–593 (1969)
56. Wu, H.-D., Barnes, F.S.: Doped $Ba_{0.6}Sr_{0.4}TiO_3$ thin films for microwave device applications at room temperature. Integ. Ferroelectr. **22**(1–4), 291–305 (1998)
57. Yoon, K.H., Lee, J.C., Park, J., Kang, D.H., Song, C.M., Seo, Y.G.: Electrical properties of Mg doped $(Ba_{0.5}Sr_{0.5})TiO_3$ thin films. Jap. J. Appl. Phys. **40**(12), 5497–5500 (2001)